NASA TECHNICAL NOTE

NASA TN D-3408

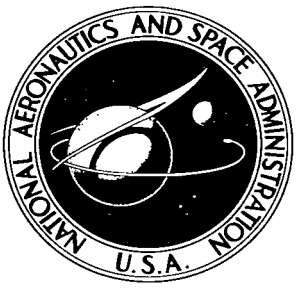

SUPERSONIC INVESTIGATION OF EFFECTS OF CONFIGURATION GEOMETRY ON PRESSURE-COEFFICIENT AND SECTION NORMAL-FORCE-COEFFICIENT DISTRIBUTIONS FOR A TWO-STAGE LAUNCH VEHICLE

by James A. Blackwell, Jr.

Langley Research Center
Langley Station, Hampton, Va.

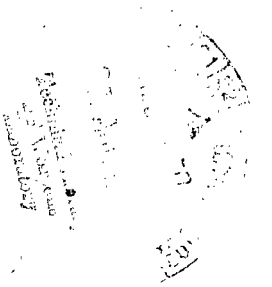

NATIONAL AERONAUTICS AND SPACE ADMINISTRATION • WASHINGTON, D. C. • AUGUST 1966

NASA TN D-3408

SUPERSONIC INVESTIGATION OF EFFECTS OF CONFIGURATION GEOMETRY ON PRESSURE-COEFFICIENT AND SECTION NORMAL-FORCE-COEFFICIENT DISTRIBUTIONS FOR A TWO-STAGE LAUNCH VEHICLE

By James A. Blackwell, Jr.

Langley Research Center
Langley Station, Hampton, Va.

NATIONAL AERONAUTICS AND SPACE ADMINISTRATION

For sale by the Clearinghouse for Federal Scientific and Technical Information
Springfield, Virginia 22151 – Price $2.00

SUPERSONIC INVESTIGATION OF EFFECTS OF CONFIGURATION GEOMETRY ON PRESSURE-COEFFICIENT AND SECTION NORMAL-FORCE-COEFFICIENT DISTRIBUTIONS FOR A TWO-STAGE LAUNCH VEHICLE

By James A. Blackwell, Jr.
Langley Research Center

SUMMARY

A wind-tunnel investigation was conducted over a Mach number range from 1.60 to 2.86 to determine the pressure-coefficient and section normal-force-coefficient distributions for a two-stage launch vehicle with variations in nose-cone angle and bluntness, upper-stage fineness ratio, and transition-flare angle. The Reynolds number of the investigation was 2.50×10^6 per foot (8.20×10^6 per meter), and the angle of attack varied generally from about -6^o to 6^o in 3^o increments. The results of the investigation indicate that increasing the nose-cone angle resulted in increases in the positive pressure coefficients and in the positive section normal-force coefficients over the nose cone. Variations in the pressure-coefficient and section normal-force-coefficient distributions resulting from variations in the nose-cone angle were generally restricted to the nose cone and to a region within about two upper-stage diameters downstream of the nose-cone—upper-stage juncture. The effects of blunting the nose cone on the pressure-coefficient and section normal-force-coefficient distributions appear to be generally restricted to the blunted region of the nose cone. The variations in pressure-coefficient and section normal-force-coefficient distributions resulting from varying the upper-stage fineness ratio are generally confined to the upper stage and the forward portion of the transition flare. Increases in the transition-flare angle are accompanied by increases in the positive pressure coefficients and in the positive section normal-force coefficients over the transition flare. For an increase in Mach number the positive pressure coefficients over the nose cones and transition flares decrease, the negative pressure coefficients over the upper stage decrease, and the pressure-coefficient distributions become flat. Variation of Mach number does not appreciably affect the section normal-force loadings over the nose cones; however, the positive section normal-force coefficients on the upper stage and transition flare are generally reduced as Mach number is increased.

INTRODUCTION

In the structural design of launch-vehicle systems, several factors concerning the aerodynamic forces or loads that the vehicle experiences during its flight must be considered. One factor is the static-pressure-coefficient distribution on the launch vehicle, which must be known to determine the optimum positions for vent locations for the launch-vehicle inner compartments in order to prevent local rupture. The maximum pressure differential producing rupture may occur at supersonic Mach numbers or at transonic Mach numbers, depending on the venting arrangements. A second factor that must be considered in the structural design of launch vehicles is the section normal-force-coefficient distribution over the launch vehicle. These forces must be known to design the launch-vehicle structure adequately to withstand the aerodynamic forces and moments experienced by the vehicle. The maximum aerodynamic bending and shear loads experienced by the launch vehicle generally occur for the condition of maximum dynamic pressure, which for most trajectories occurs in the supersonic speed range.

As part of a general program to determine the static aerodynamic characteristics of simulated launch vehicles, the present investigation was undertaken to determine the effect of variations in nose-cone angle and nose-cone bluntness, upper-stage fineness ratio, and transition-flare angle on the supersonic pressure-coefficient and section normal-force-coefficient distributions for a two-stage launch vehicle. Results indicating the effect of systematic variations in launch-vehicle geometry on the transonic pressure-coefficient and section normal-force-coefficient distributions are presented in references 1 and 2 for the same configurations used in this investigation.

The investigation was conducted in the Langley Unitary Plan wind tunnel over a Mach number range from 1.60 to 2.86. The Reynolds number of the investigation was 2.50×10^6 per foot (8.20×10^6 per meter). The angle of attack varied generally from about -6° to 6° in 3° increments.

SYMBOLS

The units used for the physical quantities defined in this paper are given in both U.S. Customary Units and in the International System of Units (SI). The SI Units are in parentheses. Factors relating the two systems are given in reference 3.

Coefficients and symbols used in this paper are defined as follows:

C_p pressure coefficient, $\frac{p - p_\infty}{q_\infty}$

c_n	body-section normal-force coefficient, $\int_0^1 \left(C_{p,l} - C_{p,u}\right) d\left(\frac{y}{r}\right)$
D	local diameter, in. (cm)
M	Mach number
p	local static pressure, psf (kN/m^2)
p_∞	free-stream static pressure, psf (kN/m^2)
q_∞	free-stream dynamic pressure, psf (kN/m^2)
r	local radius, in. (cm)
R	Reynolds number per unit length, ft^{-1} (m^{-1})
x	model station, measured from a point located 50 in. (127 cm) forward of model base, in. (cm)
y	lateral distance, measured from center line of model, in. (cm)
α	nominal angle of attack of model center line (does not include corrections for deflection of model and support system due to load), deg
δ_N	nose-cone half-angle, deg
δ_F	transition-flare half-angle, deg
ϕ	orifice-row meridian angle, positive measured counterclockwise from vertical as viewed from front, deg (see fig. 1)

Subscripts:

l	lower
max	maximum
u	upper

APPARATUS AND MODEL

Apparatus

The investigation was conducted in the low supersonic speed test section of the Langley Unitary Plan wind tunnel. The test section is 4 feet (122 cm) square and approximately 7 feet (213 cm) in length. The nozzle leading to the test section is of the asymmetric sliding block type, which allows the Mach number to be varied continuously through a range from 1.5 to 2.86. Further details of the wind tunnel may be found in reference 4.

Model surface pressures were measured by using six automatic scanning units which incorporate strain-gage-type pressure transducers of various pressure ranges to permit attainment of maximum accuracy.

Model

General dimensions of the model and of associated interchangeable components are presented in figure 1. For this investigation, the model components of figure 1 were arranged in 10 configurations which are described in figure 2 and table 1. The configurations tested in this investigation were identical to those reported in reference 1, and the same configuration nomenclature is used. As a result, the configuration numbers do not always follow an orderly progression as far as model geometric variations are concerned.

Model pressure orifices were generally installed along four longitudinal rows which were located at meridian angles ϕ (positive measured counterclockwise from the vertical as viewed from the front) of 0°, -30°, -60°, and -90°, respectively. (See fig. 1.) The two configurations utilizing blunted conical noses (6 and 7) had a single, closely spaced orifice row ($\phi = 0^{\circ}$) on the nose portion and four rows rearward from the nose-cone—upper-stage juncture. All longitudinal orifice positions are referenced to model station 0. (See fig. 2.)

TESTS AND PROCEDURES

The test conditions are summarized in the following table:

M	q_∞,		R,	
	psf	kN/m^2	per ft	per m
1.60	601	28.8	2.50×10^6	8.20×10^6
2.00	592	28.3	2.50	8.20
2.36	560	26.8	2.50	8.20
2.86	492	23.5	2.50	8.20

Results were obtained for the model upright and for the model rolled 15° clockwise, as viewed from the front, over an angle-of-attack range from -6° to 6°. Through the proper combination of data from various test conditions, it was possible to simulate the pressure distribution around the launch vehicle at angles of attack of 3° and 6°. These results were then machine integrated in order to obtain the launch-vehicle section normal-force coefficients.

The investigation was conducted with boundary-layer transition fixed by means of a circumferential transition strip located at the nose-cone—upper-stage corner. The transition strip was 0.100 inch (0.254 cm) wide and was composed of No. 60 carborundum grains set in a plastic adhesive.

CORRECTIONS AND ACCURACY

Angles of attack not corrected for deflection of the model and support system under load are referred to as nominal angles of attack. The nominal angles of attack, however, have been corrected for tunnel airflow angularity. The accuracy of the nominal angles of attack presented herein, not including the uncertainty due to model and support deflection, is estimated to be ±0.1°. Since the true angle of attack is the nominal angle of attack plus the correction for deflection of the model and support system under load, an approximation of the model deflection under load has been made from results obtained from static loadings of the test model and support system. Results of the static loadings are shown in figure 3 for loads applied at three model stations. Based upon normal-force and center-of-pressure results for similar configurations (ref. 5) and results of the static loadings from figure 3, an additional deflection (in the direction of the resultant normal force) of less than 0.15° would be expected for the maximum-loading condition of the present investigation.

At supersonic speeds, the experimental results are affected by boundary-reflected disturbances produced by the model; these disturbances occur at Mach numbers from slightly over 1.0 to those at which the disturbances are reflected downstream of the model base. For the present investigation, the results for the following model stations are affected by boundary-reflected disturbances:

Configuration	M	α, deg	Model station	
			x, in.	x, cm
1	1.60	6	40 to 50	101.6 to 127.0
	1.60	-6	47 to 50	119.4 to 127.0
2	1.60	6	36 to 50	91.4 to 127.0
	1.60	-6	42 to 50	106.7 to 127.0
	1.60	3	48 to 50	121.9 to 127.0
3 through 10	1.60	6	31 to 50	78.7 to 127.0
	1.60	-6	38 to 50	96.5 to 127.0
	1.60	3	44 to 50	111.8 to 127.0
	1.60	-3	47 to 50	119.4 to 127.0
	2.00	6	39 to 50	99.1 to 127.0
	2.00	-6	45 to 50	114.3 to 127.0
	2.36	6	47 to 50	119.4 to 127.0

A consideration of factors affecting the results of this investigation has indicated general inaccuracies in pressure coefficient to be of the order of ± 0.01. However, in model regions of extremely varying pressures or for conditions where pressures are noticeably sensitive to small Mach number changes, greater inaccuracies may be expected. Local deviations from the quoted free-stream Mach numbers did not exceed ± 0.015.

RESULTS

Results of this investigation were obtained in the form of pressure coefficients and sectional normal-force coefficients. Complete tabulations of the pressure coefficients and the section normal-force coefficients are too voluminous to be of general interest and are presented separately in a "Supplement to NASA TN D-3408, 1966" that may be obtained upon request.[1]

Representative data have been selected for presentation herein (figs. 4 to 11) and are plotted to show general effects of the configuration variables on the pressure coefficients and section normal-force coefficients (multiplied by a diameter ratio) at various angles of attack and Mach numbers. Schlieren photographs of similar models without pressure orifices are provided in figure 12 to indicate the effect of varying transition-flare angle.

[1]Address requests to Full-Scale Research Division, NASA Langley Research Center, Langley Station, Hampton, Va. 23365.

DISCUSSION

Pressure-Coefficient Distributions

In general, an overall change is noted in the shape of the pressure-coefficient distribution over the launch vehicle as the Mach number is increased. At transonic speeds (ref. 1) and at low supersonic speeds (e.g., M = 1.60, fig. 4) there are noticeable pressure recoveries associated with the pressure-coefficient peaks over the upper stage and transition flare. As the speed is increased to high supersonic Mach numbers (e.g., M = 2.86, fig. 4), the pressure-coefficient distributions tend to become flat, and the pressure-coefficient peaks resulting from the expansion and compression corners disappear.

Effect of nose-cone angle.- The effects of increasing nose-cone angle on the pressure-coefficient distributions are presented in figure 4. These results show that an increase in nose-cone angle results in an increase in the positive pressure coefficients over the nose cone. In addition, an increase in nose-cone angle increases the negative pressure coefficients at and just rearward of the nose-cone—upper-stage juncture at Mach numbers 1.60 and 2.00. At Mach numbers 2.36 and 2.86, a change in the nose-cone angle has only a slight effect on the pressure coefficients at and rearward of the nose-cone—upper-stage juncture, which indicates to what extent the downstream influence resulting from varying the nose-cone angle decreases with increase in Mach number. This effect is probably slight because the peak negative pressure coefficient at the nose-cone—upper-stage juncture is a function of the vacuum pressure coefficient (pressure coefficient corresponding to an absolute local pressure of zero) which decreases with increase in Mach number. For instance, the vacuum pressure coefficient at Mach number 1.6 is approximately -0.558 and at Mach number 2.86 is approximately -0.174. It is also interesting to note that the carryover effect from varying the nose-cone angle on the pressure coefficients of the upper stage extends only approximately 2 upper-stage diameters rearward of the nose-cone—upper-stage juncture. The effect of increasing Mach number at supersonic speeds on the pressure coefficients over the nose cone is to decrease the values of the positive pressure coefficients. This trend is in agreement with that predicted by theory for cones as presented in reference 6. At transonic speeds reference 1 shows that, as the Mach number is increased transonically until the shock wave attaches to the nose, the positive pressure coefficients over the nose cone increase, which is opposite to the trend noted herein for an increase in supersonic Mach number.

The effects of angle of attack on the pressure coefficients over the nose cone can be seen by comparing figures 4(a), 4(b), and 4(e) for a representative orifice-row-orientation angle of 0°. These results indicate that as the angle of attack is increased from -6° to 6° the positive pressure coefficients at $\phi = 0^{\circ}$ generally decrease. The variation in

pressure coefficient over the nose cone due to angle of attack is generally larger for orifices that are windward than for orifices that are on the leeward side of the nose cone.

Effect of nose bluntness.- Results showing the effects of blunting the forward portion of the 22.5° half-angle nose cone are presented in figure 5. The main effects of blunting the nose appear to be highly localized; they are generally restricted to the blunted region of the nose cone.

Effect of upper-stage fineness ratio.- The effects of variations in upper-stage fineness ratio on the launch-vehicle pressure-coefficient distribution are presented in figure 6. These results indicate that the main effects of varying the upper-stage fineness ratio are confined to the upper stage and the forward portion of the transition flare. For the lowest upper-stage fineness ratio (1.42) the compression wave (which causes an increase in positive pressure coefficient) at the upper-stage—transition-flare juncture seems somewhat attenuated. This attenuation probably develops because the low-pressure region resulting from the nose cone interferes with the pressure field over the transition flare.

The effects of angle of attack on the pressure coefficients on the upper stage can be seen by comparing figures 6(a), 6(b), and 6(c) for $\phi = 0^{\circ}$. The results indicate that the general effect of increasing the angle of attack at $\phi = 0^{\circ}$ is to increase the negative pressure coefficients over the upper stage. However, at a Mach number of 1.60, the pressure coefficients at $\phi = 0^{\circ}$ on the upper stage (from approximately 1.5 upper-stage diameters rearward of the nose-cone—upper-stage juncture to the upper-stage—transition-flare juncture) tend to increase positively with increase in angle of attack. This effect is more pronounced for the largest upper-stage fineness ratio (4.85). This result can also be found at transonic Mach numbers. (See refs. 1 and 7.)

The effect of increasing Mach number (fig. 6) is generally to decrease the negative pressure coefficients over the upper stage.

Effect of transition-flare angle.- Pressure-coefficient results obtained for various transition-flare angles are shown in figure 7. Increases in transition-flare angle generally result in increases in the positive pressure coefficients over the transition flare for all test Mach numbers. Variations in the negative pressure coefficients at and just rearward of the transition-flare—main-stage corner due to increases in the transition-flare angle generally follow trends similar to those which were shown previously for variations in nose-cone angle. The carryover effect from varying the transition-flare angle on the pressure coefficients of the main stage extends approximately 1.75 main-stage diameters rearward of the transition-flare—main-stage juncture. It is interesting to note that this carryover effect is most noticeable at the sonic (ref. 1) and low supersonic Mach numbers ($M = 1.6$ and $M = 2.0$). The effects on the pressure-coefficient distribution forward of the transition flare due to changes in the flare angle can be seen to vary

widely. For the 5° transition flare (configuration 3) and for the 15° transition flare (configuration 8), no effects on the upper-stage—pressure-coefficient distribution forward of the transition flare are noticed. However, for the 10.1° transition flare a compression is seen to occur from approximately $1\frac{1}{2}$ to 2 upper-stage diameters forward of the transition flare. Schlieren photographs taken of similar models with no pressure orifices are presented in figure 12 for the various flare angles. From the schlieren photographs for the 10.1° flare (configuration 10) and the data for all roll angles, no reason is apparent for the compression forward of the transition flare (fig. 7). The 30° transition flare (configuration 9) affects the upper-stage—pressure-coefficient distribution approximately 0.75 upper-stage diameter forward of the transition flare. This effect is a result of flow separation forward of the 30° transition flare. (See schlieren photographs in fig. 12.)

For an increase in angle of attack at $\phi = 0^\circ$ or Mach number (fig. 7) the positive pressure coefficients over the transition flare generally decrease, which is a similar result to that obtained for variations of the pressure coefficients over the nose cone with Mach number and angle of attack.

Section Normal-Force-Coefficient Distributions

Effect of nose-cone angle.- The effects of nose-cone angle on the launch-vehicle section normal-force coefficients are shown in figure 8. These results indicate that, generally, effects of variations in nose-cone angle on the section normal-force coefficients are restricted to the nose cone and to a region within about 2 upper-stage diameters downstream of the nose-cone—upper-stage juncture. The results tend to indicate a nearly linear increase in loading with increasing distance rearward from the apex of the nose cone for configurations 4 and 5. This linearity is as would be expected, since theory (ref. 8) for slightly yawed cones predicts a constant pressure coefficient over the nose cone in the x-direction for a constant meridian angle ϕ and these coefficients, when integrated and multiplied by D/D_{max}, yield a linear increase in section loads. Sufficient orifices were not available near the nose-cone apex to indicate this effect for configuration 3. The results also show that the maximum nose-cone section normal-force coefficients, which occur just forward of the nose-cone base, increase slightly with increasing nose angle. At the nose-cone—upper-stage juncture for some of the nose cones an abrupt decrease in loading occurs. These negative loadings result because the expansion occurring at the nose-cone—upper-stage juncture begins at different points on the upper and lower surfaces. (See figs. 4(b) and 4(c).) The positive section normal-force loadings downstream of the nose-cone—upper-stage juncture are a result of the nose-cone carryover effect and tend to increase as nose-cone angle is increased. Variation of Mach number does not appreciably affect the section normal-force loadings over the nose cone; however, the carryover effect on the upper stage from the nose cone is generally reduced as Mach number is increased.

Effect of nose-cone bluntness.- The effects of variations in nose-cone bluntness on the section normal-force-coefficient distributions are shown in figure 9. It should be noted that because only a single orifice row was installed on the blunt-cone configurations, no section normal-force coefficients are available for the nose-cone portions of these configurations; that is, for model stations upstream of $x = 12.51$ in. (31.78 cm).

The main effects of nose-cone bluntness on the section normal-force coefficients presented in figure 9 appear to be restricted to the blunted region of the nose cone, since generally negligible effects are indicated downstream of the nose cone.

Effect of upper-stage fineness ratio.- In figure 10, results are presented showing the effects of varying upper-stage fineness ratio on the section normal-force-coefficient distributions. Examination of these results indicates that the section normal-force coefficients over the nose cone, the upper stage just rearward of the nose-cone—upper-stage juncture, and aft of the transition flare are only slightly affected as the upper-stage fineness ratio is reduced from 4.85 to 1.42. Notable variations in loading do occur, however, over the upper stage just ahead of the transition flare and over the transition flare as the upper-stage fineness ratio is reduced. In particular, significant positive increases in loading occur over the transition flare at Mach numbers 2.00 to 2.86 as the upper-stage fineness ratio is reduced from 2.99 to 1.42. This increase is quite interesting, since from reference 2 it can be seen that reducing the upper-stage fineness ratio tends to reduce the positive section normal-force coefficients over the transition flare at Mach numbers of 1.0 and 1.2. It should be noted that the erratic variations in the results over the main stage shown in figure 10(b) for $M = 1.60$ are caused in this vicinity by shock waves reflecting from the wind-tunnel walls, as was noted in the section entitled "Corrections and Accuracy."

For configuration 3 at a Mach number of 1.60 the section normal-force coefficients over the rearward portion of the upper stage can be seen to be substantially negative (fig. 10). This trend is a result of the positive pressure coefficients on the upper surface increasing in this vicinity with increasing angle of attack, as was noted previously.

Effect of transition-flare angle.- In figure 11, the effects of varying the transition-flare half-angle on the distributed section normal-force coefficients are presented. For the Mach numbers and angles of attack of this investigation, notable positive section normal-force coefficients are developed over the transition flares. From figure 11, it can be seen that increases in transition-flare angle generally are accompanied by increases in the transition-flare positive section normal-force coefficients. For the 30° transition-flare configuration, sizable negative section normal-force coefficients occur immediately upstream of the transition-flare—upper-stage juncture as a result of the local separation. The positive section normal-force coefficients over the main-stage cylinder following the transition flares are a result of the transition-flare load carryover

and are only slightly affected by variation in transition-flare angle. Increasing the Mach number generally tends to reduce the positive section normal-force coefficients over the transition flare.

CONCLUDING REMARKS

A wind-tunnel investigation has been conducted at supersonic speeds to determine the static-pressure-coefficient and section normal-force-coefficient distributions on simulated two-stage launch vehicles. The results of the investigation indicate the following:

1. Increasing the nose-cone angle resulted in increases in the positive pressure coefficients and increases in the positive section normal-force coefficients over the nose cone. Variations in the pressure-coefficient and section normal-force-coefficient distributions resulting from variations in the nose-cone angle were generally restricted to the nose cone and to a region within about 2 upper-stage diameters downstream of the nose-cone—upper-stage juncture.

2. The effects of blunting the nose cone on the pressure-coefficient and section normal-force-coefficient distributions appear to be generally restricted to the blunted region of the nose cone.

3. The effects of varying the upper-stage fineness ratio on the pressure-coefficient and section normal-force-coefficient distributions are generally confined to the upper stage and the forward portion of the transition flare.

4. Increases in the transition-flare angle generally are accompanied by increases in the positive pressure coefficients and increases in the positive section normal-force coefficients over the transition flare.

5. For an increase in Mach number, the positive pressure coefficients over the nose cones and transition flares decrease, the negative pressure coefficients over the upper stage decrease, and the pressure-coefficient distributions become flat. Variation of Mach number does not appreciably affect the section normal-force loadings over the nose cones; however, the positive section normal-force coefficients on the upper stage and transition flare are generally reduced as Mach number is increased.

Langley Research Center,
National Aeronautics and Space Administration,
Langley Station, Hampton, Va., March 30, 1966.

REFERENCES

1. Kelly, Thomas C.: Investigation at Transonic Mach Numbers of the Effects of Configuration Geometry on Surface Pressure Distributions For a Simulated Launch Vehicle. NASA TM X-845, 1963.

2. Kelly, Thomas C.: Aerodynamic Load Distributions at Transonic Speeds for a Group of Simulated Launch-Vehicle Models. NASA TM X-1264, 1966.

3. Mechtly, E. A.: The International System of Units – Physical Constants and Conversion Factors. NASA SP-7012, 1964.

4. Anon.: Manual for Users of the Unitary Plan Wind Tunnel Facilities of the National Advisory Committee for Aeronautics. NACA, 1956.

5. Kelly, Thomas C.; and Ross, Thomas P.: Effects of Configuration Geometry on the Transonic Aerodynamic Characteristics of a Simulated Launch Vehicle. NASA TM X-976, 1964.

6. Ames Research Staff: Equations, Tables, and Charts for Compressible Flow. NACA Rept. 1135, 1953. (Supersedes NACA TN 1428.)

7. Kelly, Thomas C.: Aerodynamic Loading Characteristics at Mach Numbers From 0.80 to 1.20 of a 1/10-Scale Three-Stage Scout Model. NASA TN D-945, 1961.

8. Van Dyke, Milton D.: A Study of Second-Order Supersonic Flow Theory. NACA Rept. 1081, 1952. (Supersedes NACA TN 2200.)

TABLE 1.- MODEL CONFIGURATIONS

Configuration number	δ_N, deg	Upper-stage fineness ratio	δ_F, deg	Main-stage fineness ratio
1	22.5	1.42	5.0	7.0
2	22.5	2.99	5.0	↓
3	22.5	4.85	5.0	
4	15.3	4.85	5.0	
5	30.0	4.85	5.0	
6	[1]22.5	4.85	5.0	
7	[2]22.5	4.85	5.0	
8	22.5	6.50	15.0	
9	22.5	6.49	30.0	
10	22.5	5.79	10.1	

[1]Blunted; ratio of cap radius to cone base radius, 0.3.

[2]Blunted; ratio of cap radius to cone base radius, 0.6.

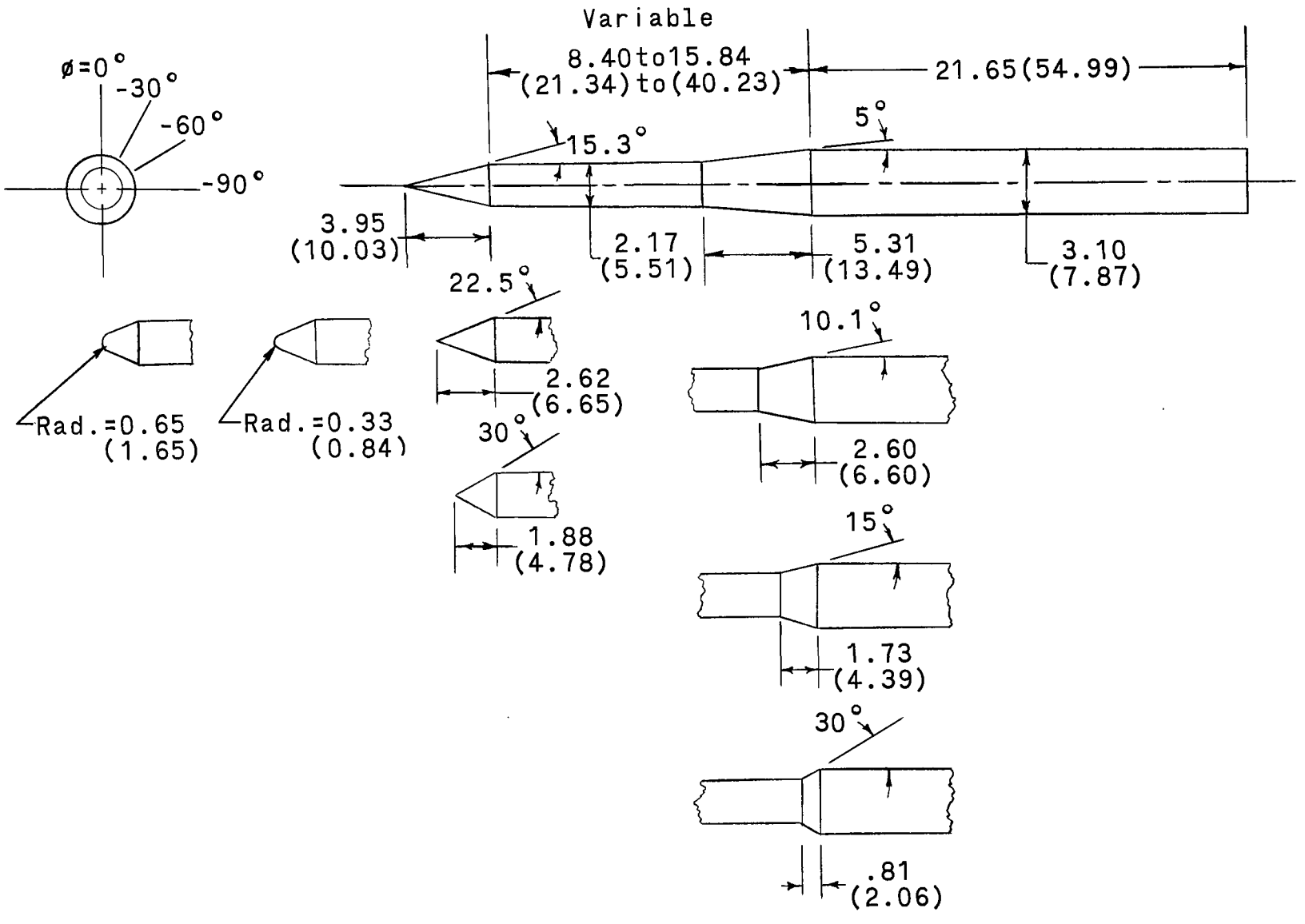

Figure 1.- Details of models. Dimensions in parentheses are in centimeters; all other dimensions in inches unless otherwise specified.

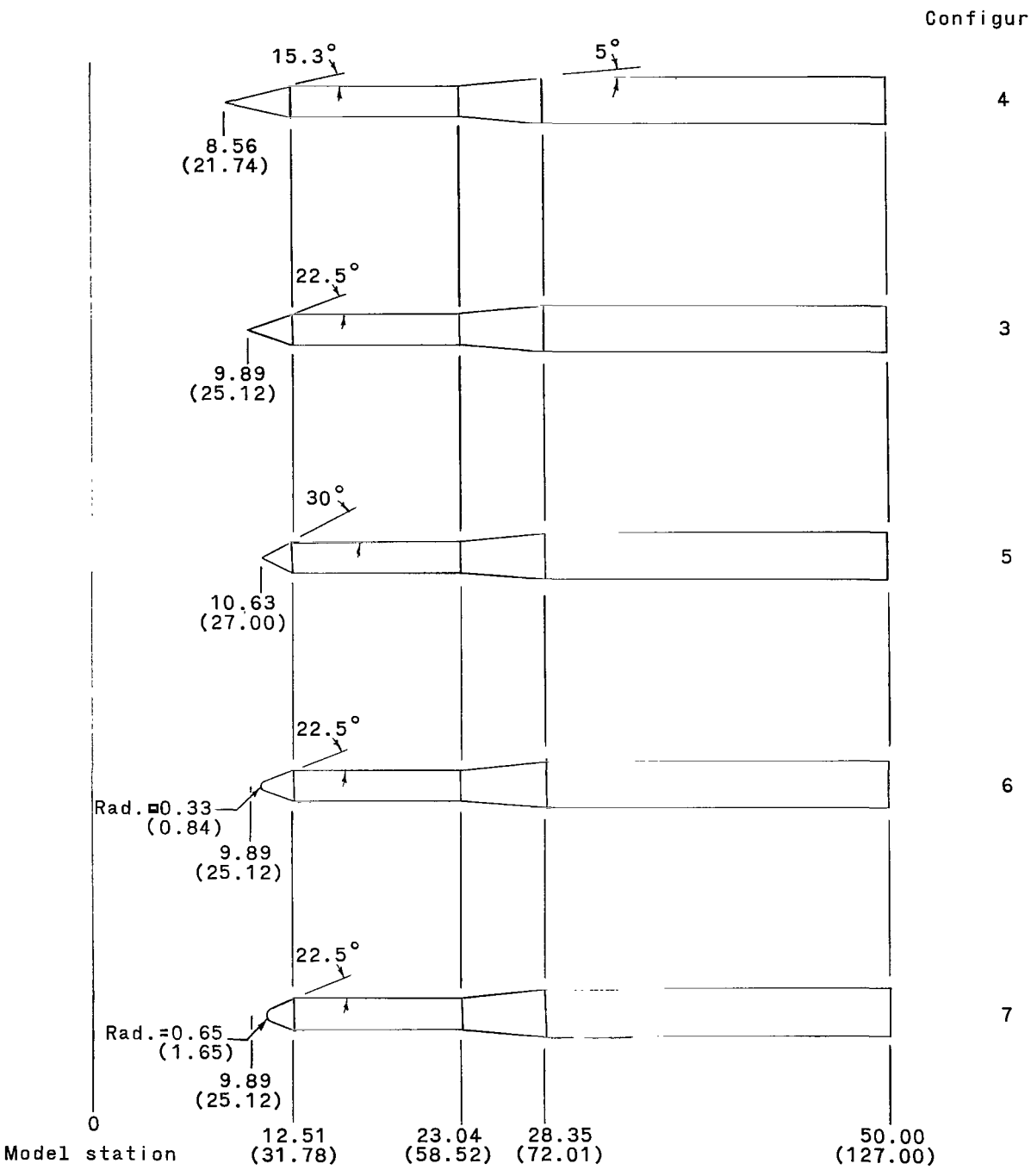

(a) Nose-cone variations.

Figure 2.- Model configurations. Model stations in parentheses are in centimeters; all other model stations in inches.

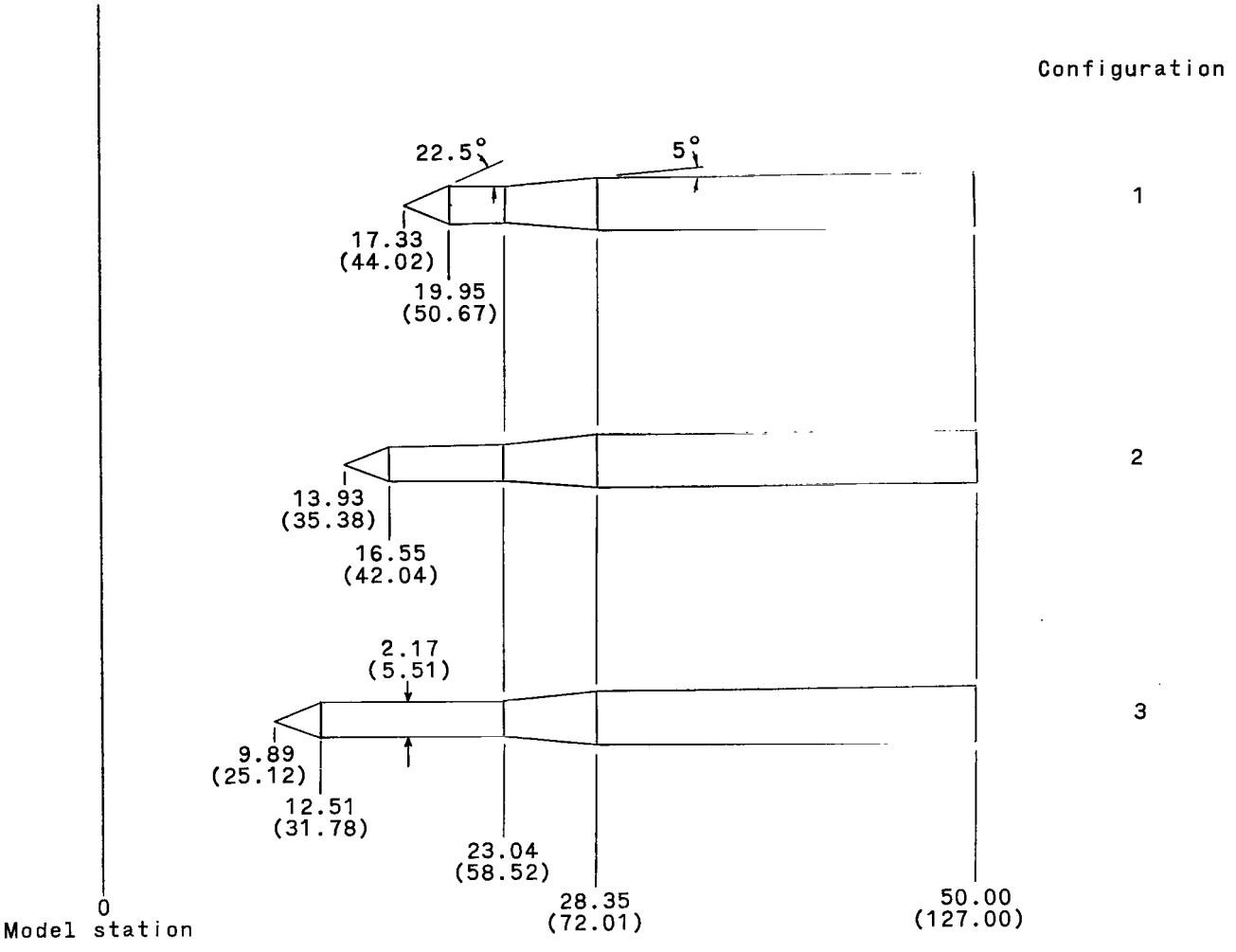

(b) Upper-stage fineness-ratio variations.

Figure 2.- Continued.

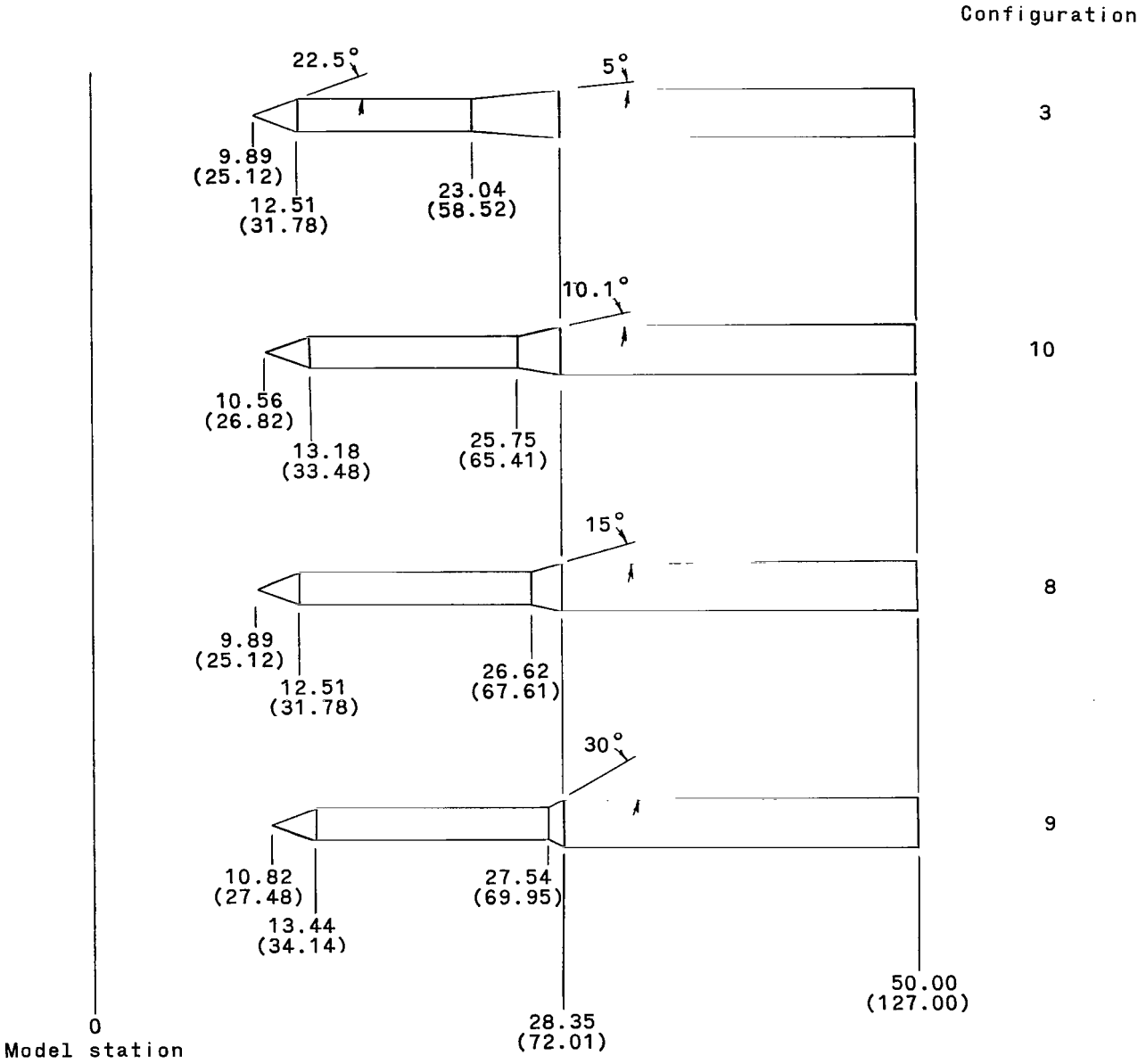

(c) Transition-flare variations.

Figure 2.- Concluded.

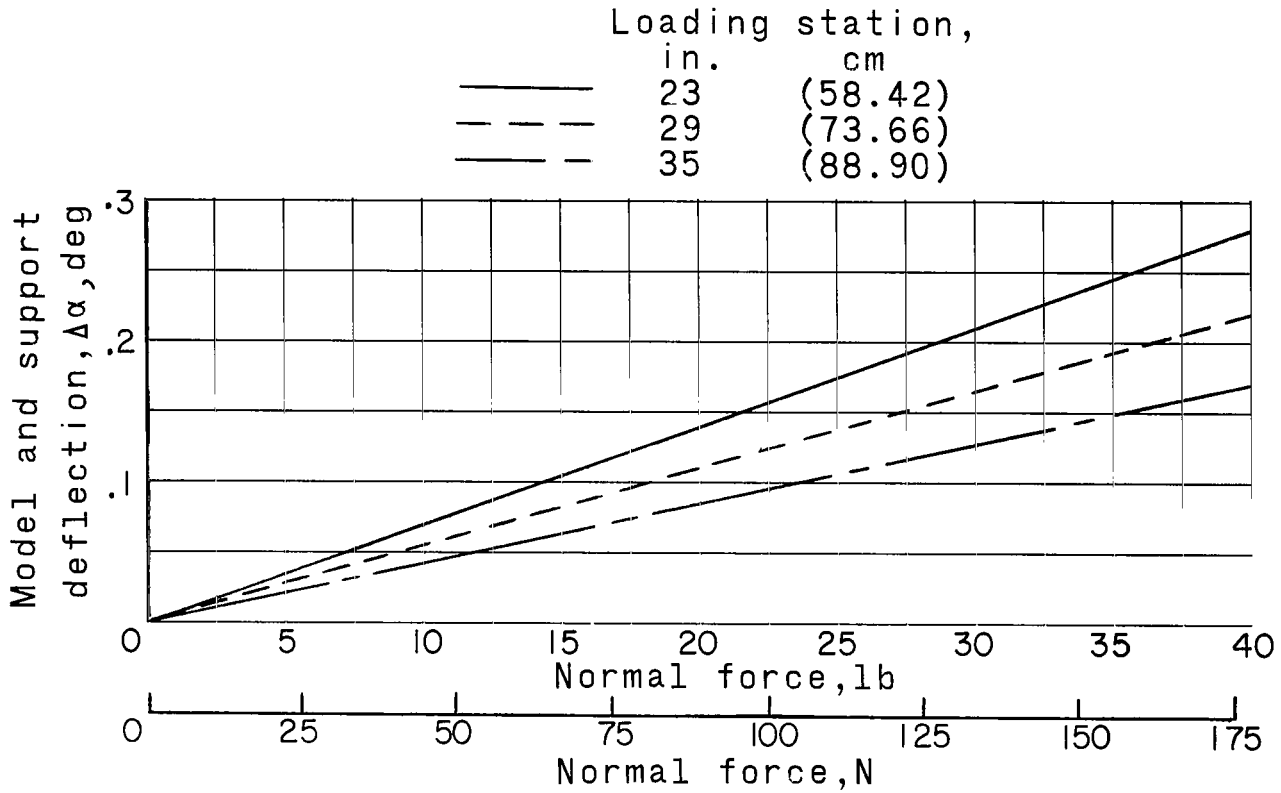

Figure 3.- Variation of model and support deflection with normal force.

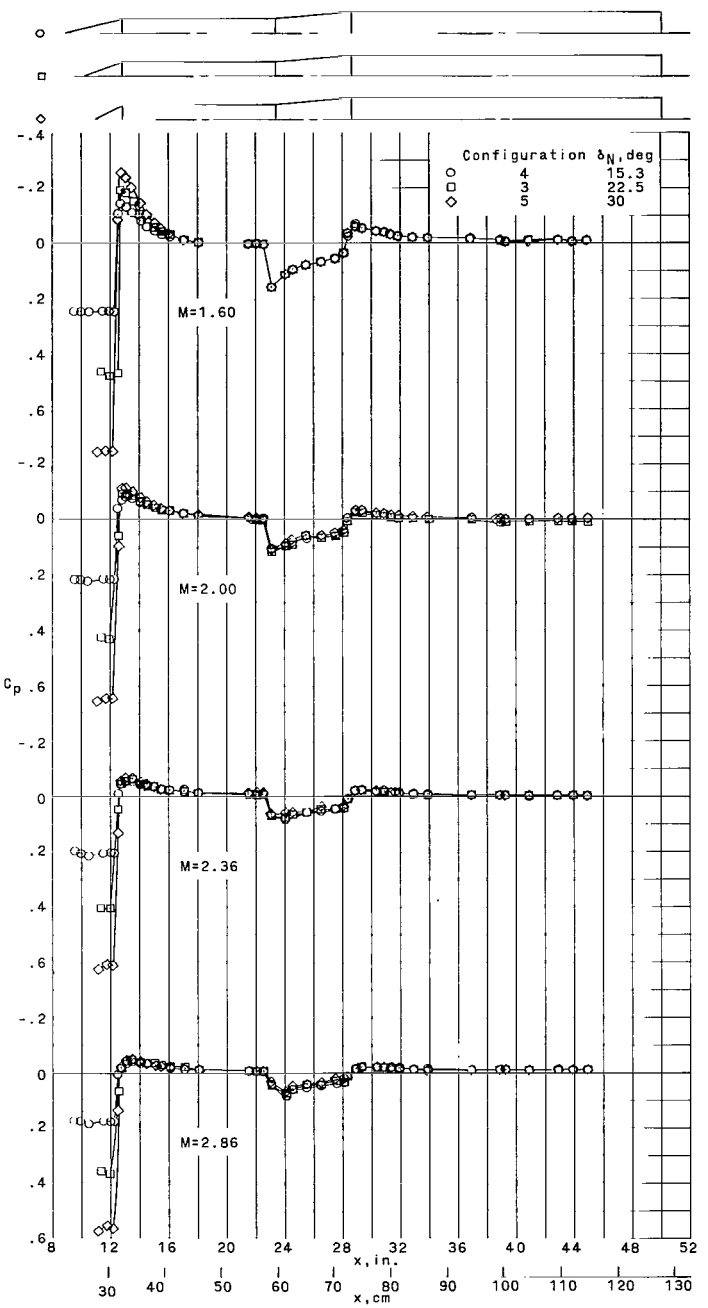

(a) $\alpha = 0^{0}$.

Figure 4.- Effects of variations in nose-cone angle on launch vehicle pressure-coefficient distribution. $\Phi = 0^{0}$; $\delta_F = 5^{0}$.

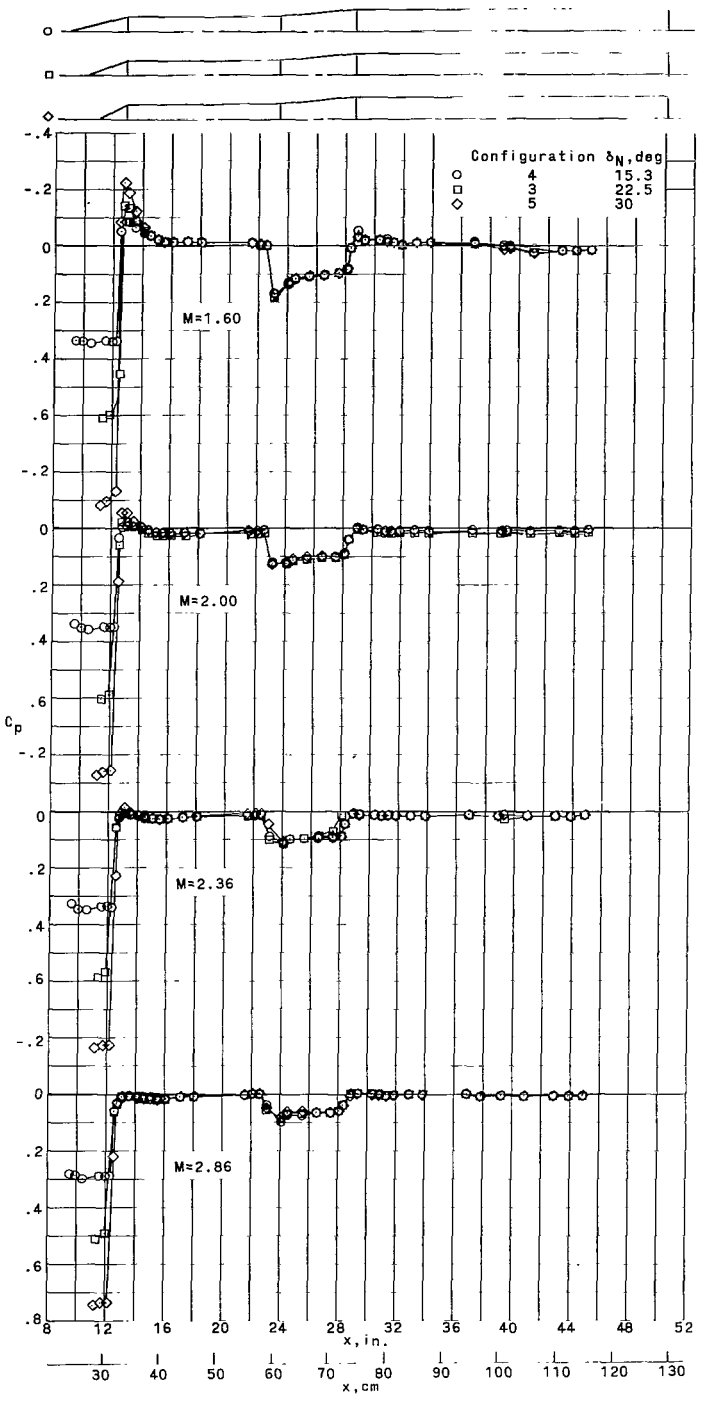

(b) $\alpha = -6^{0}$.

Figure 4.- Continued.

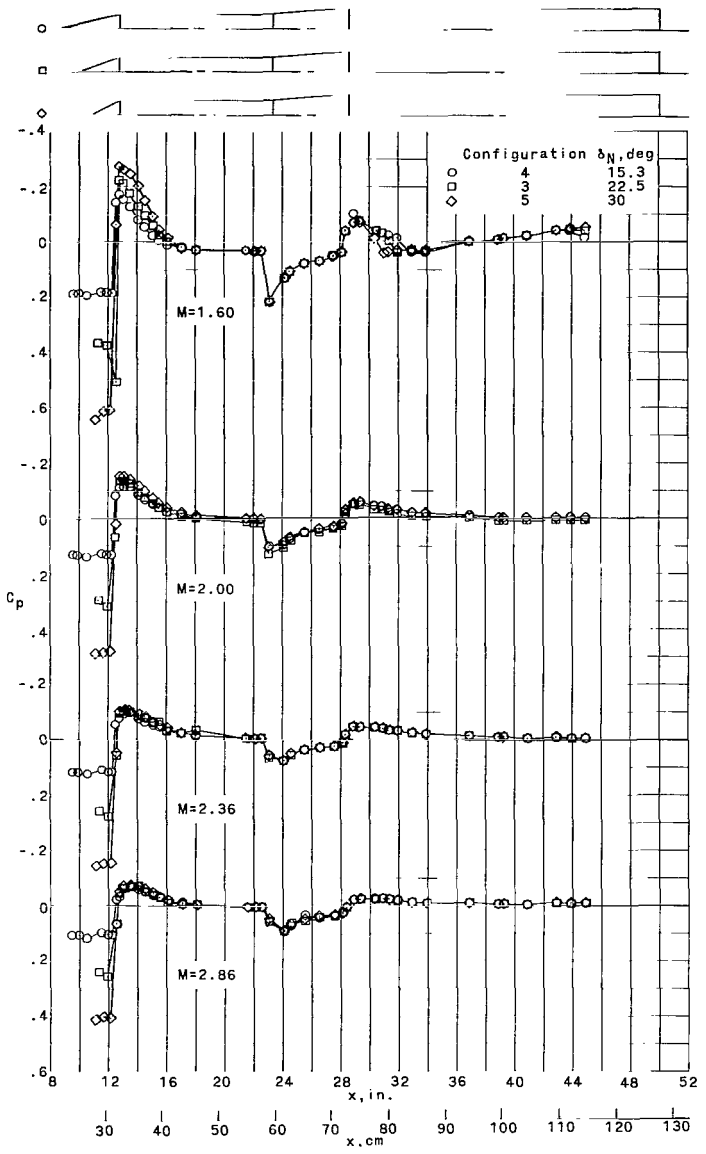

(c) $\alpha = 6^0$.

Figure 4.- Concluded.

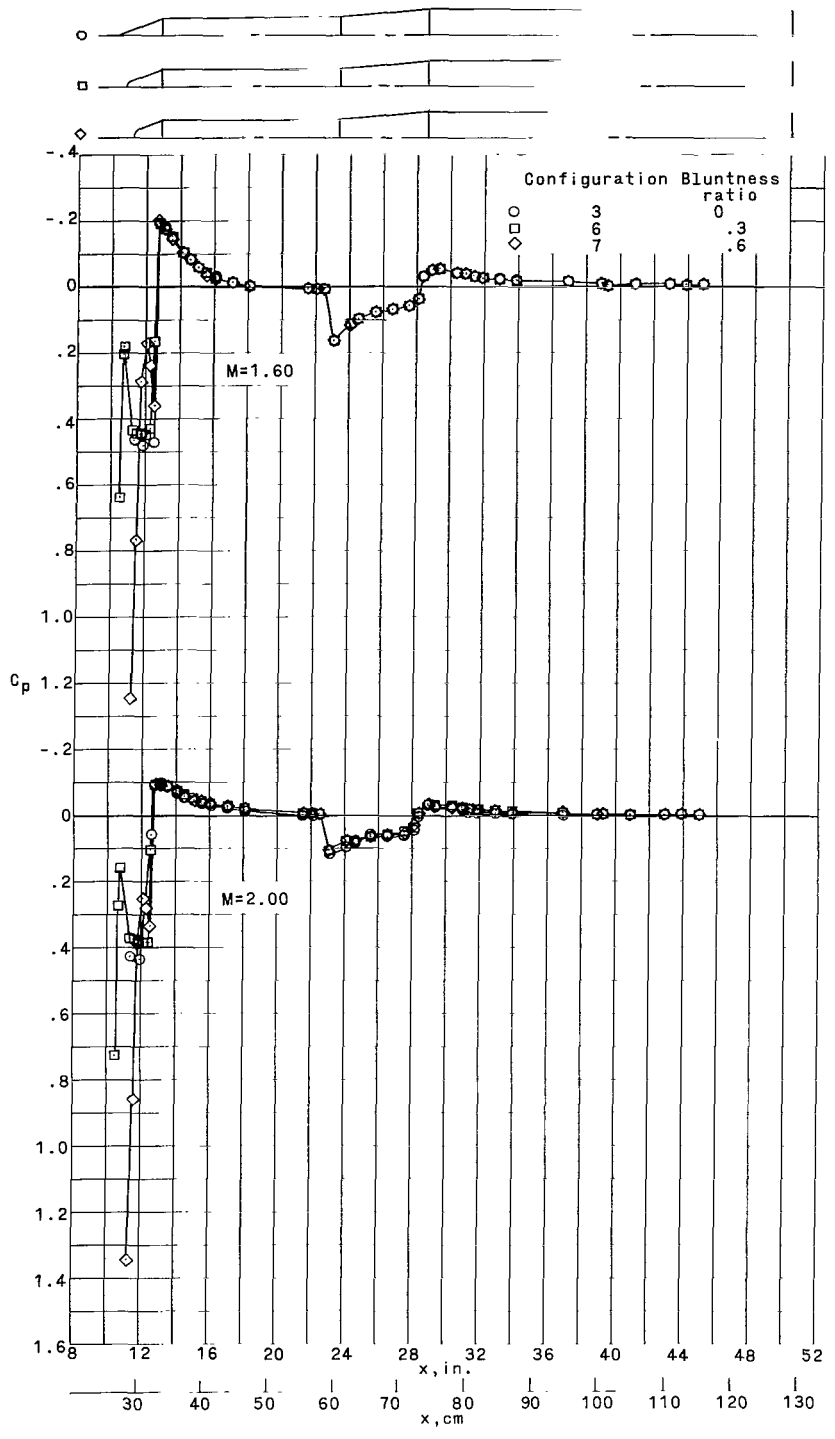

(a) $\alpha = 0^0$.

Figure 5.- Effects of nose-cone bluntness on launch vehicle pressure-coefficient distribution. $\Phi = 0^0$; $\delta_N = 22.5^0$; $\delta_F = 5^0$.

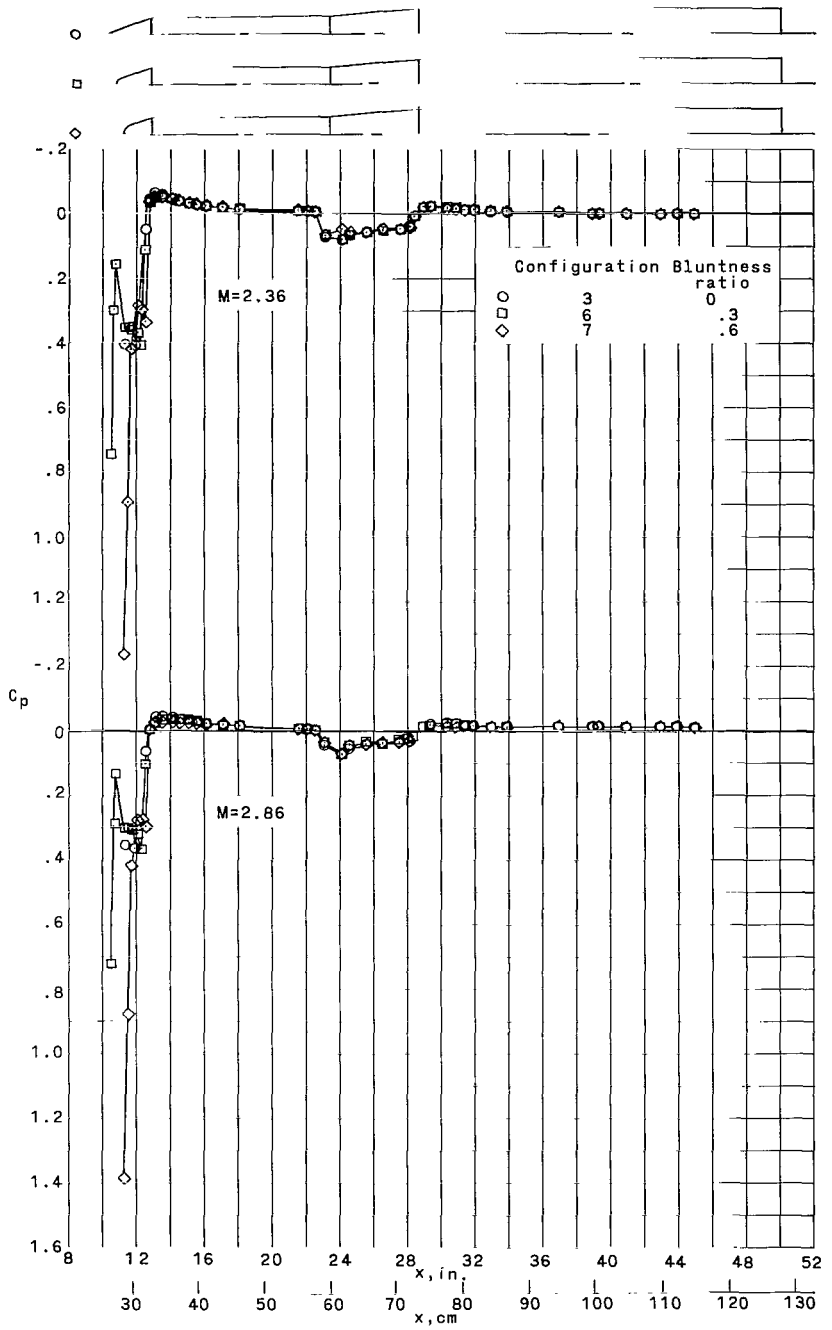

(a) Concluded.

Figure 5.- Continued.

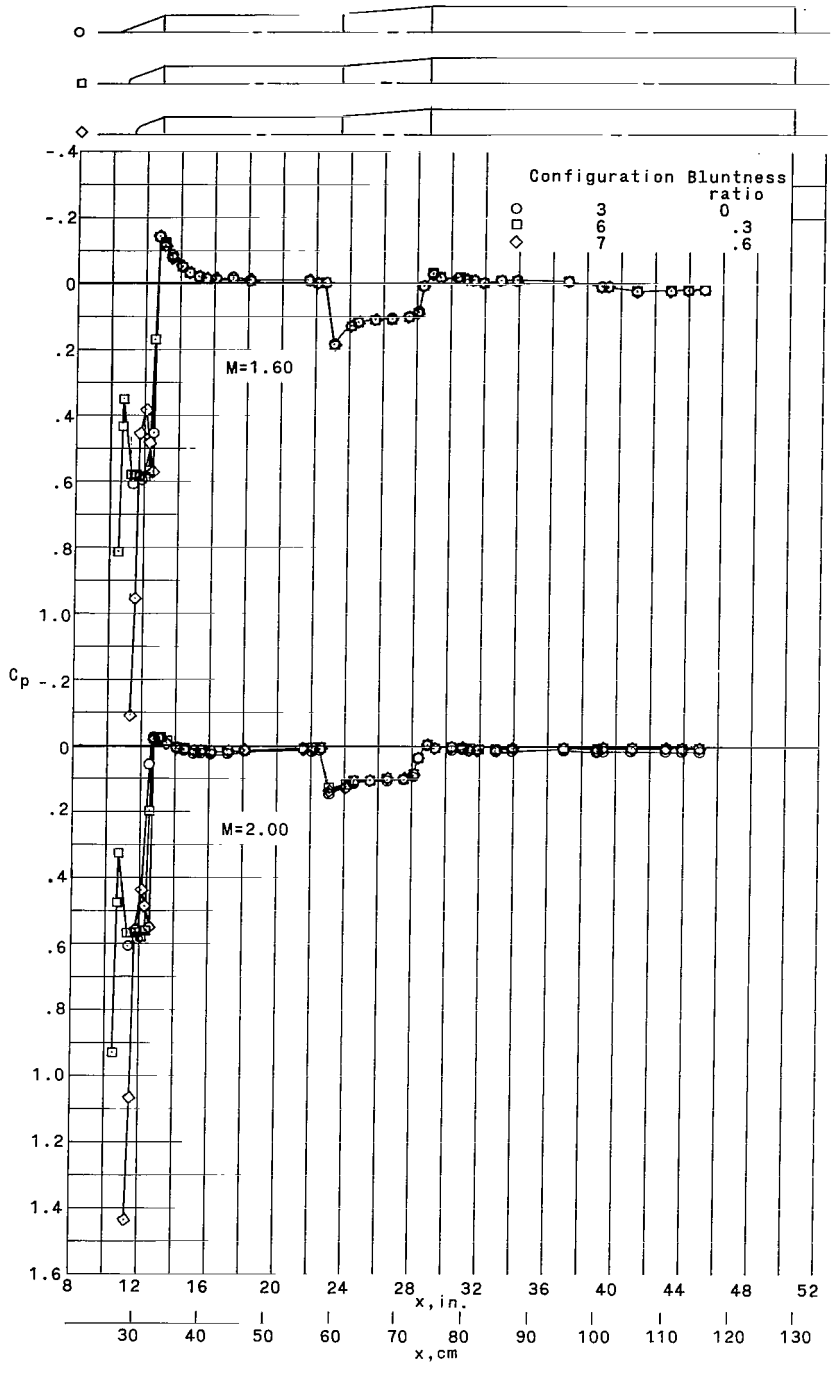

(b) $\alpha = -6^0$.

Figure 5.- Continued.

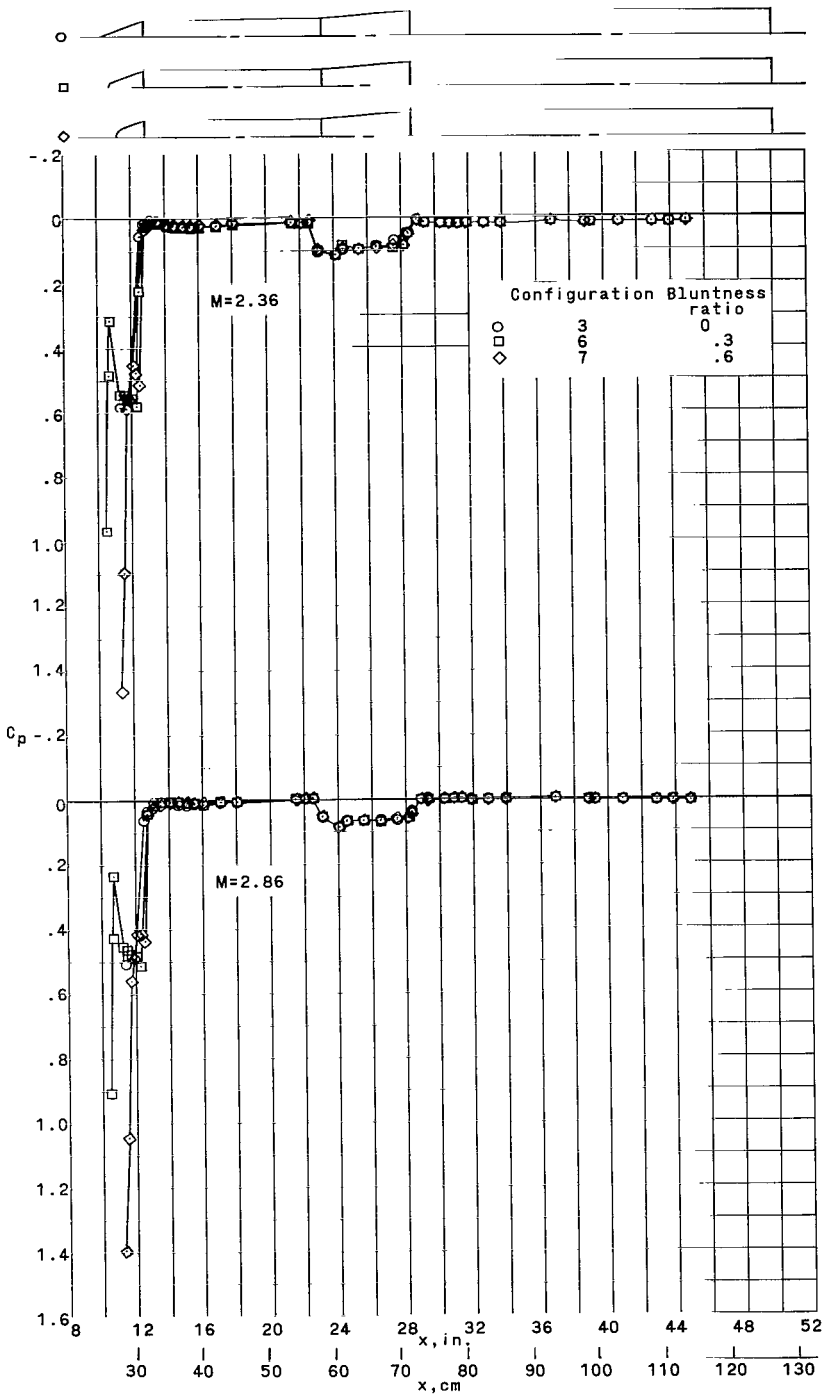

(b) Concluded.

Figure 5.- Continued.

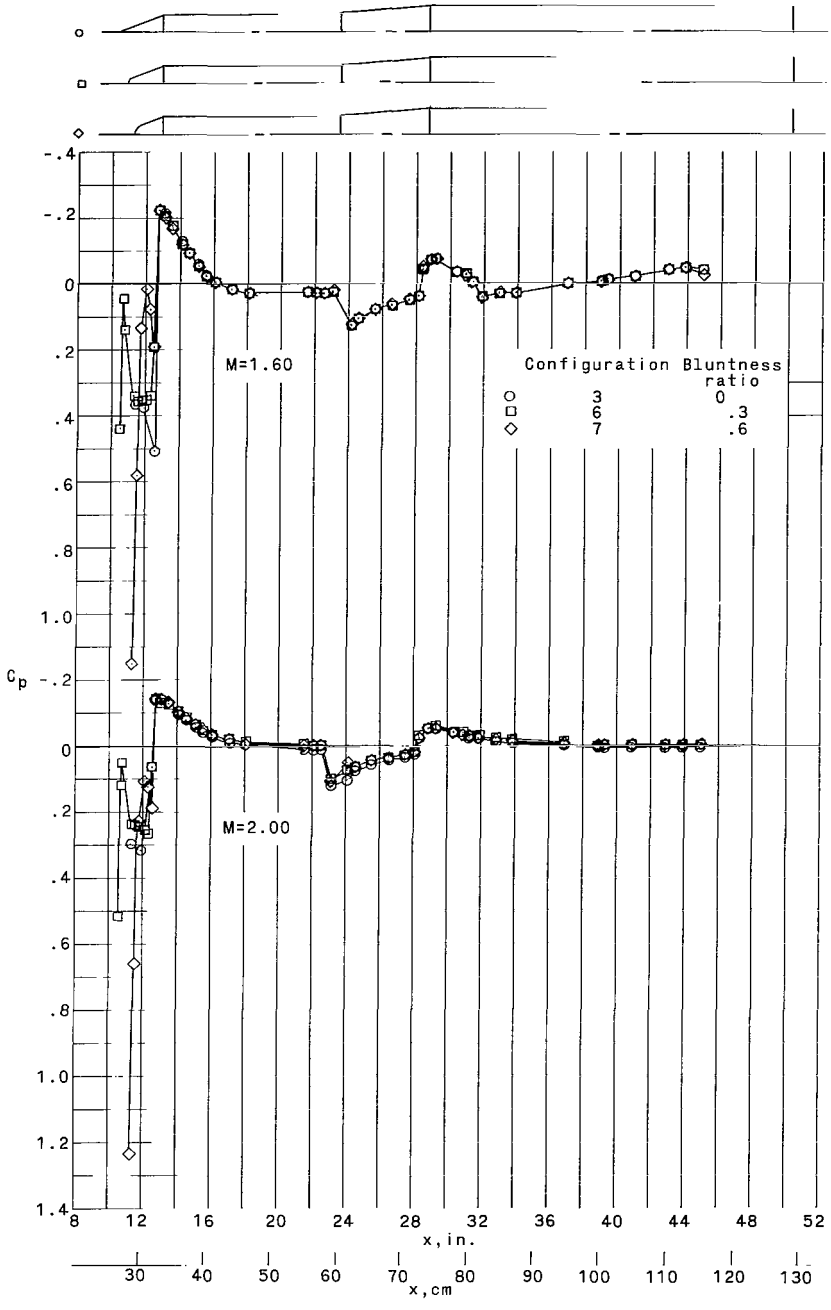

(c) $\alpha = 6^0$.

Figure 5.- Continued.

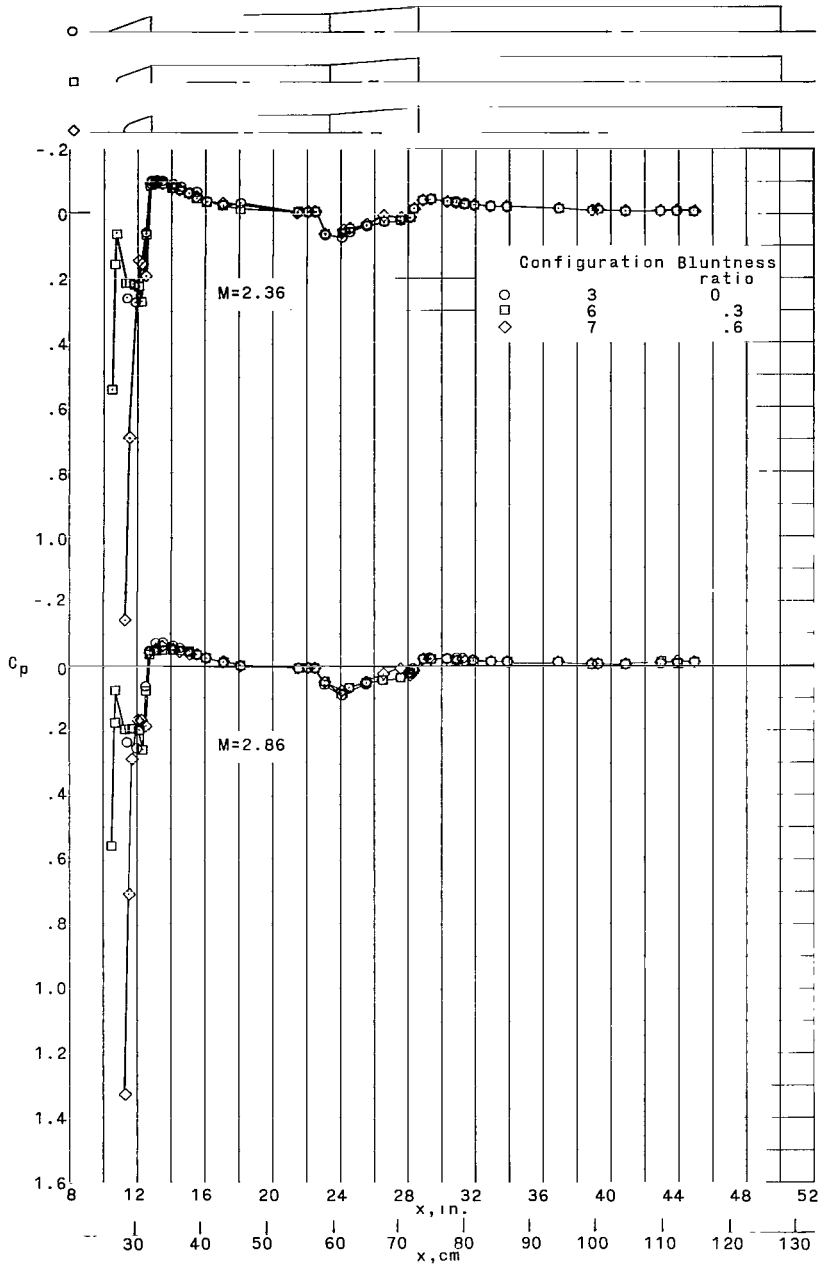

(c) Concluded.

Figure 5.- Concluded.

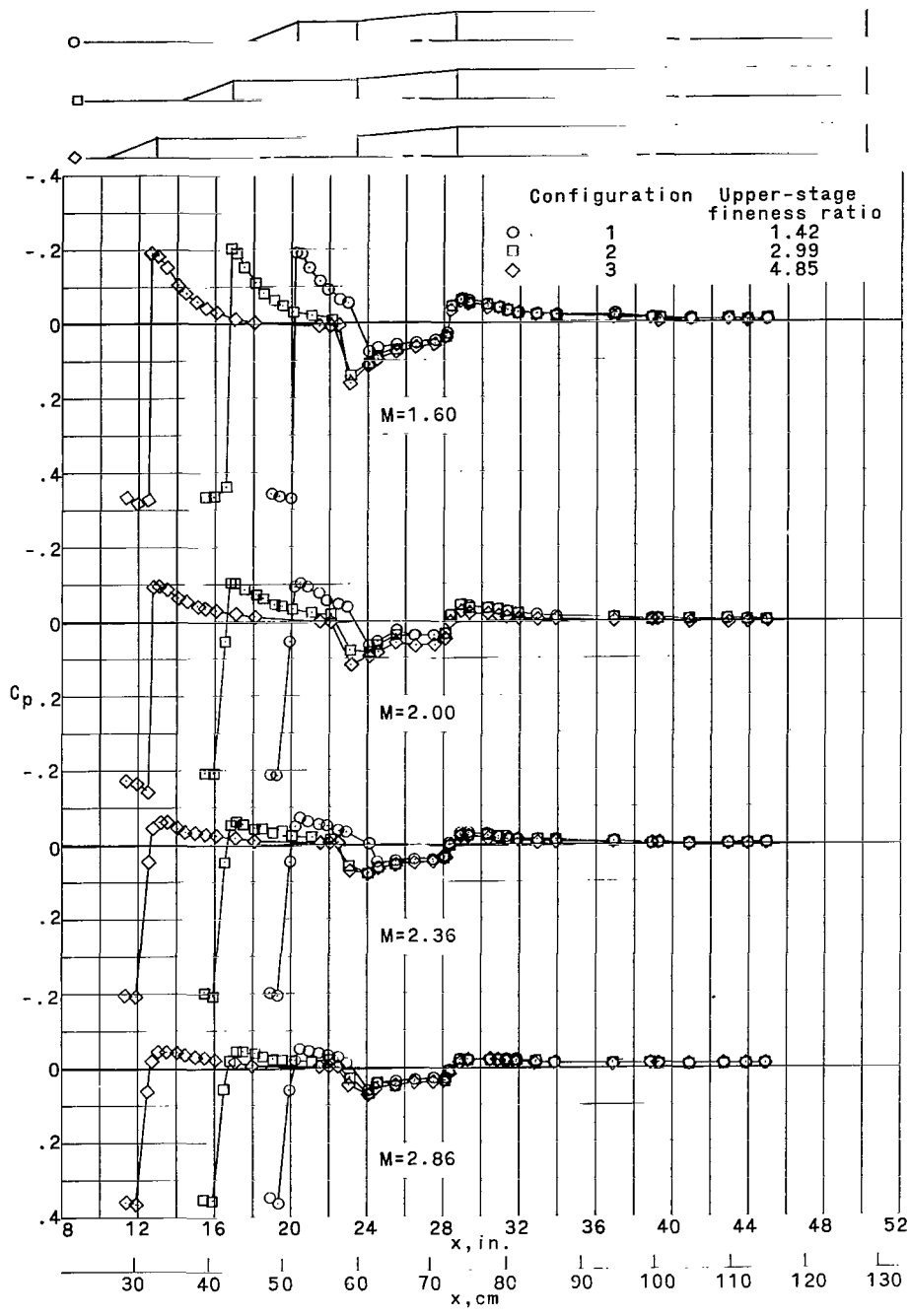

(a) $\alpha = 0^{\circ}$.

Figure 6.- Effects of variations in upper-stage fineness ratio on launch vehicle pressure-coefficient distribution. $\Phi = 0^{\circ}$; $\delta_N = 22.5^{\circ}$; $\delta_F = 5^{\circ}$.

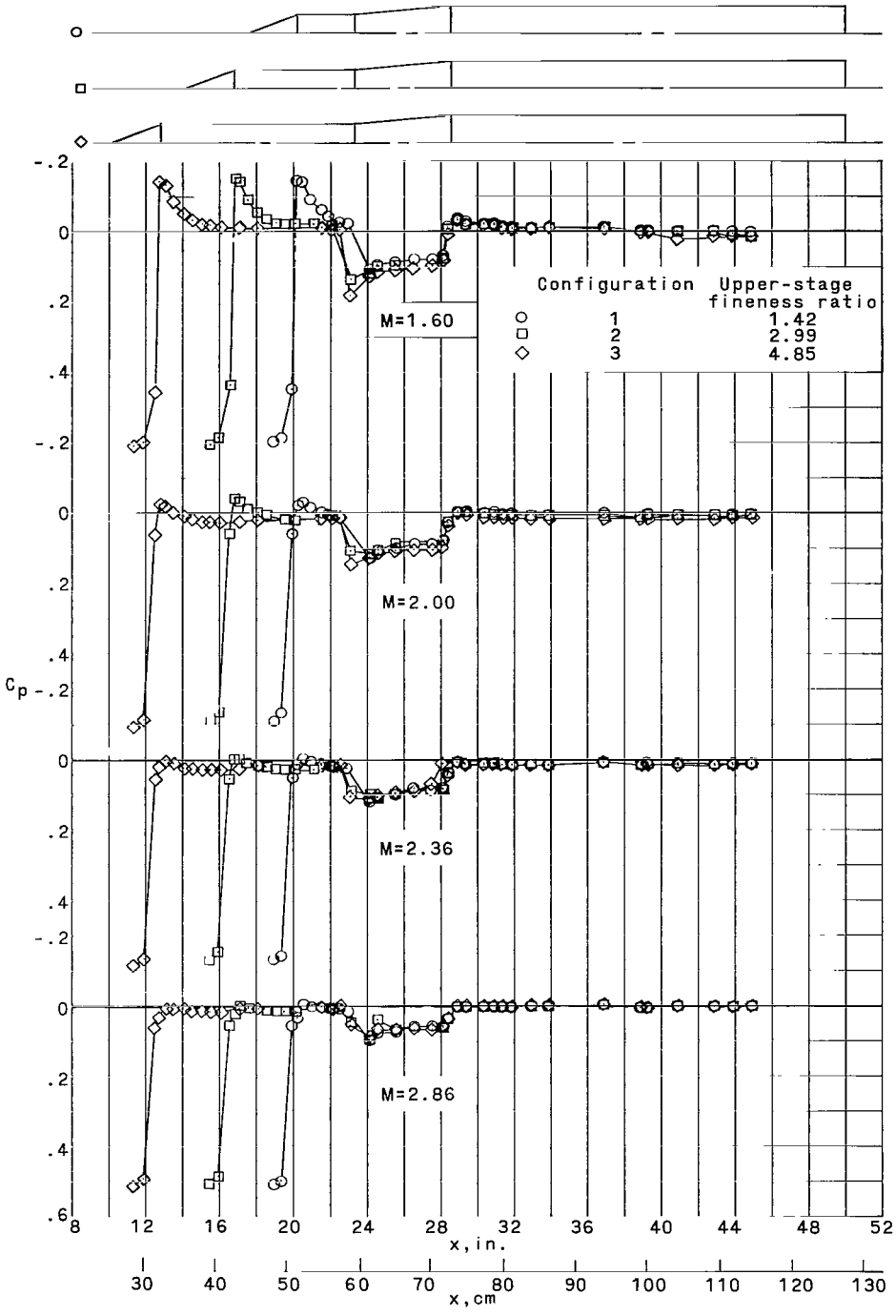

(b) $\alpha = -6^{\circ}$.

Figure 6.- Continued.

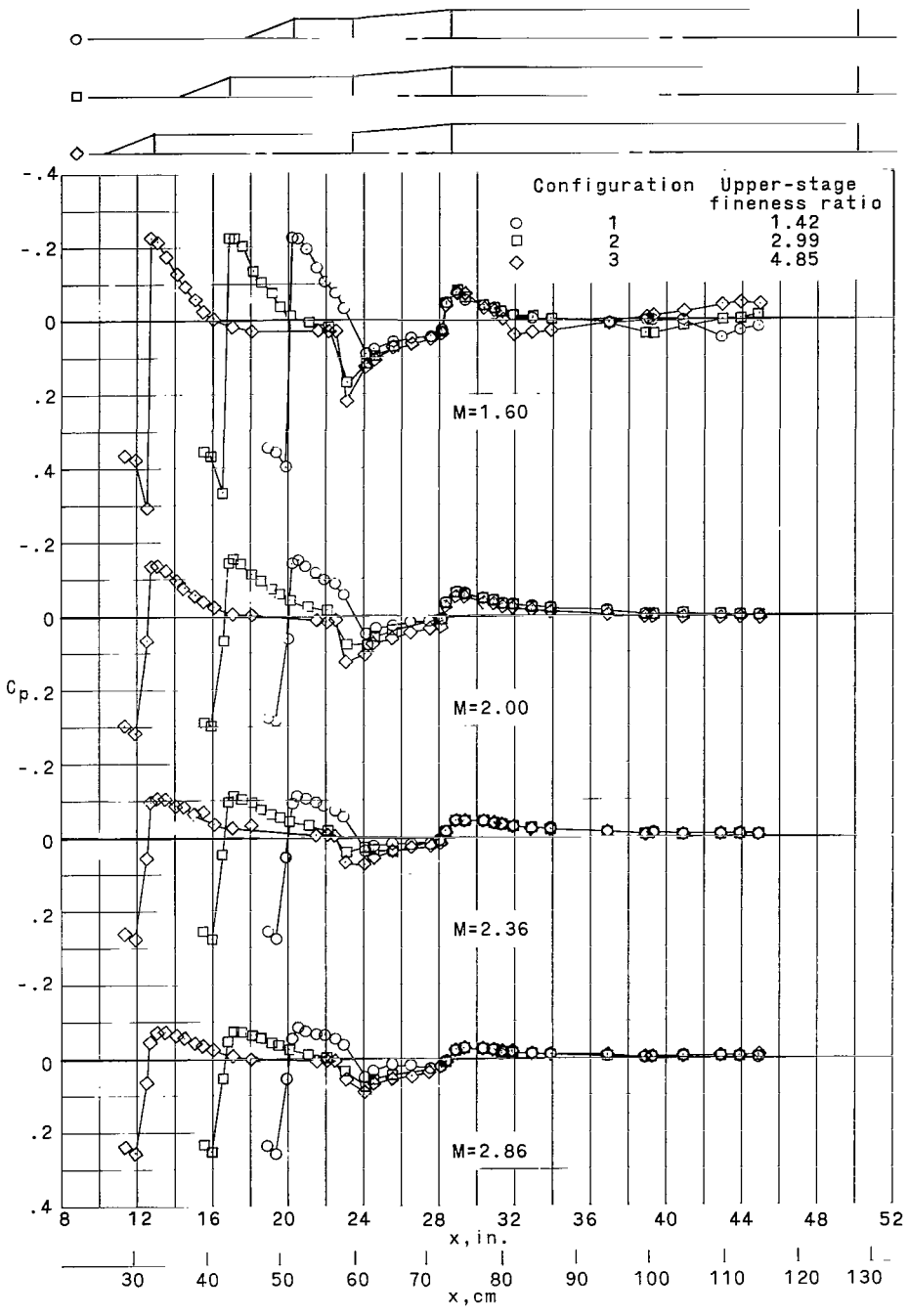

(c) $\alpha = 6^0$.

Figure 6.- Concluded.

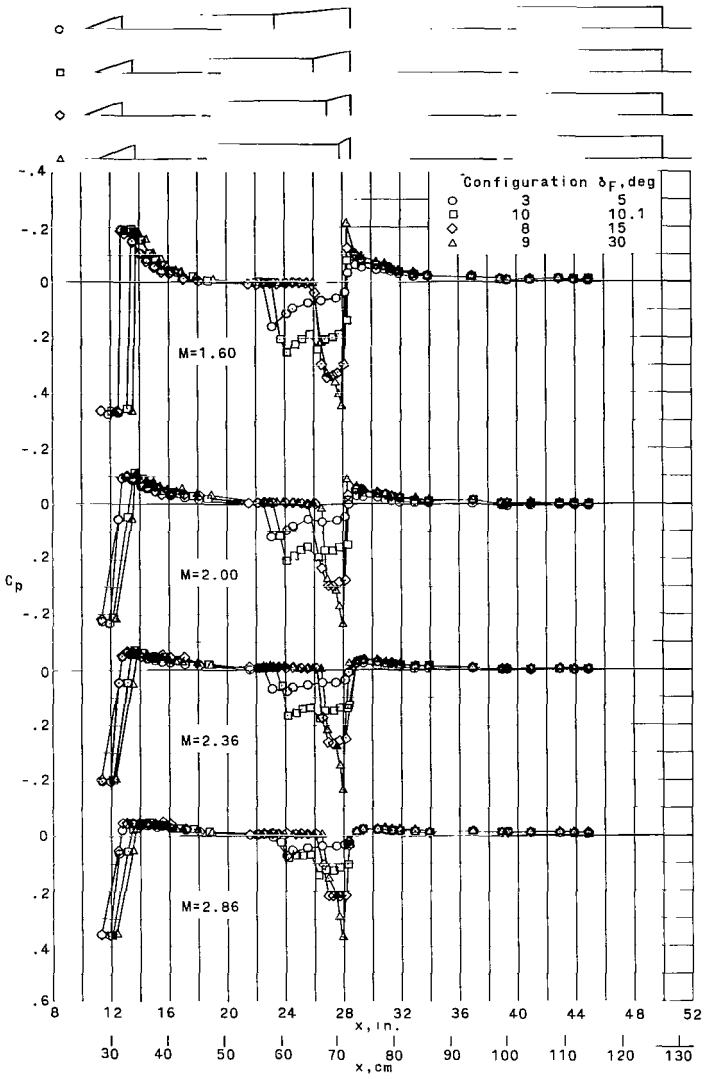

(a) $\alpha = 0^0$.

Figure 7.- Effects of variations in stage transition-flare angle on launch vehicle pressure-coefficient distribution. $\Phi = 0^0$; $\delta_N = 22.5^0$.

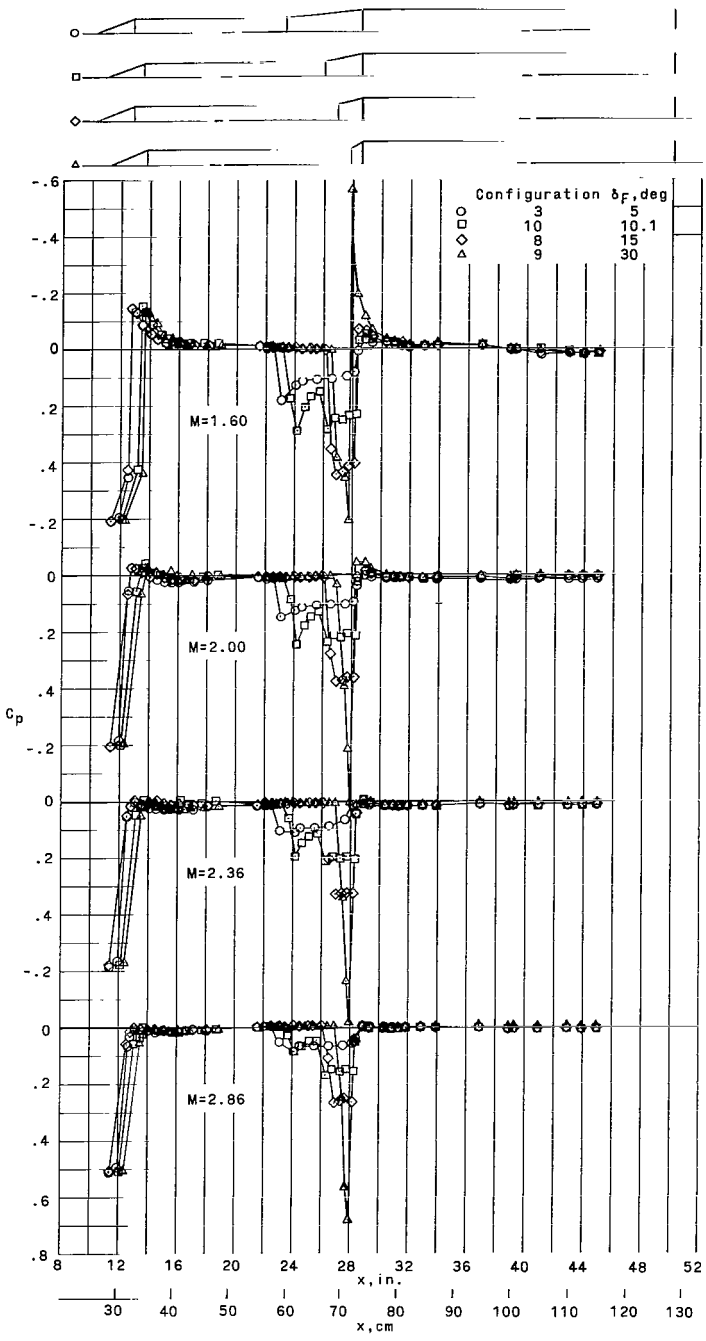

(b) $\alpha = -6^{0}$.

Figure 7.- Continued.

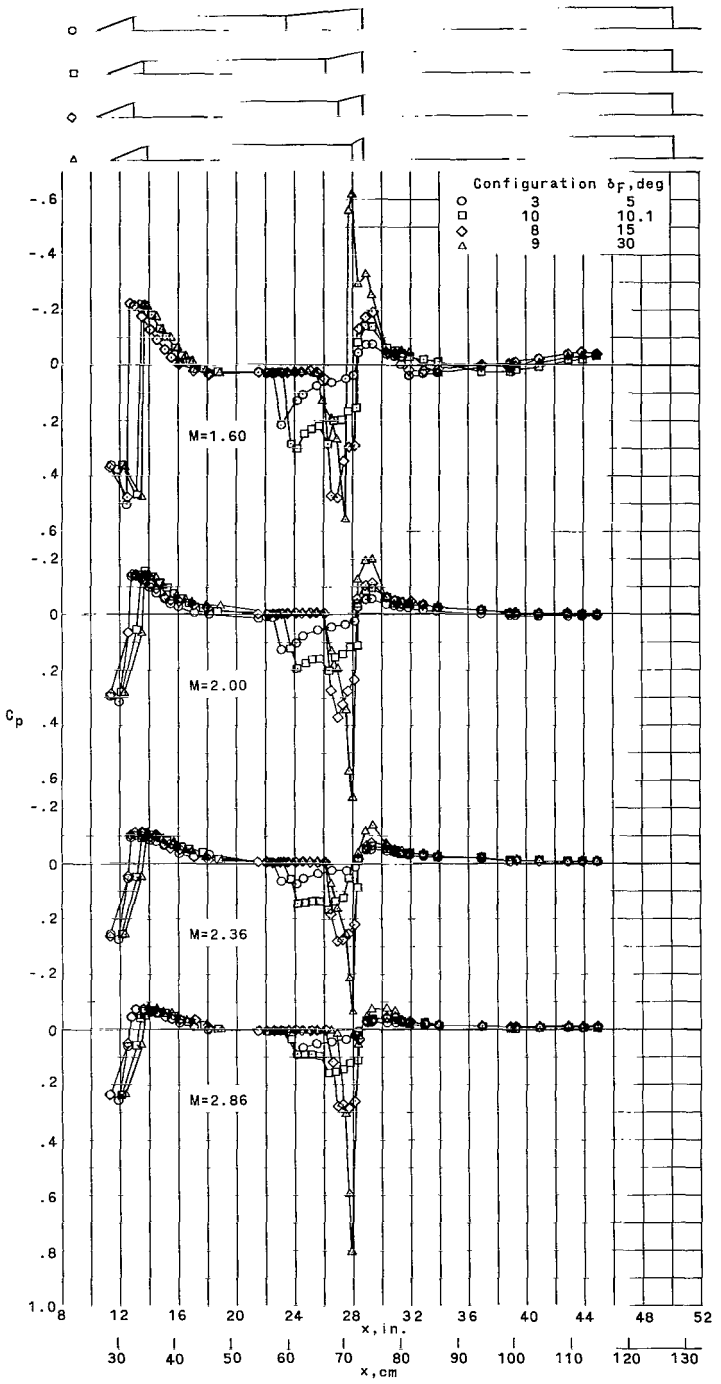

(c) $\alpha = 6^{0}$.

Figure 7.- Concluded.

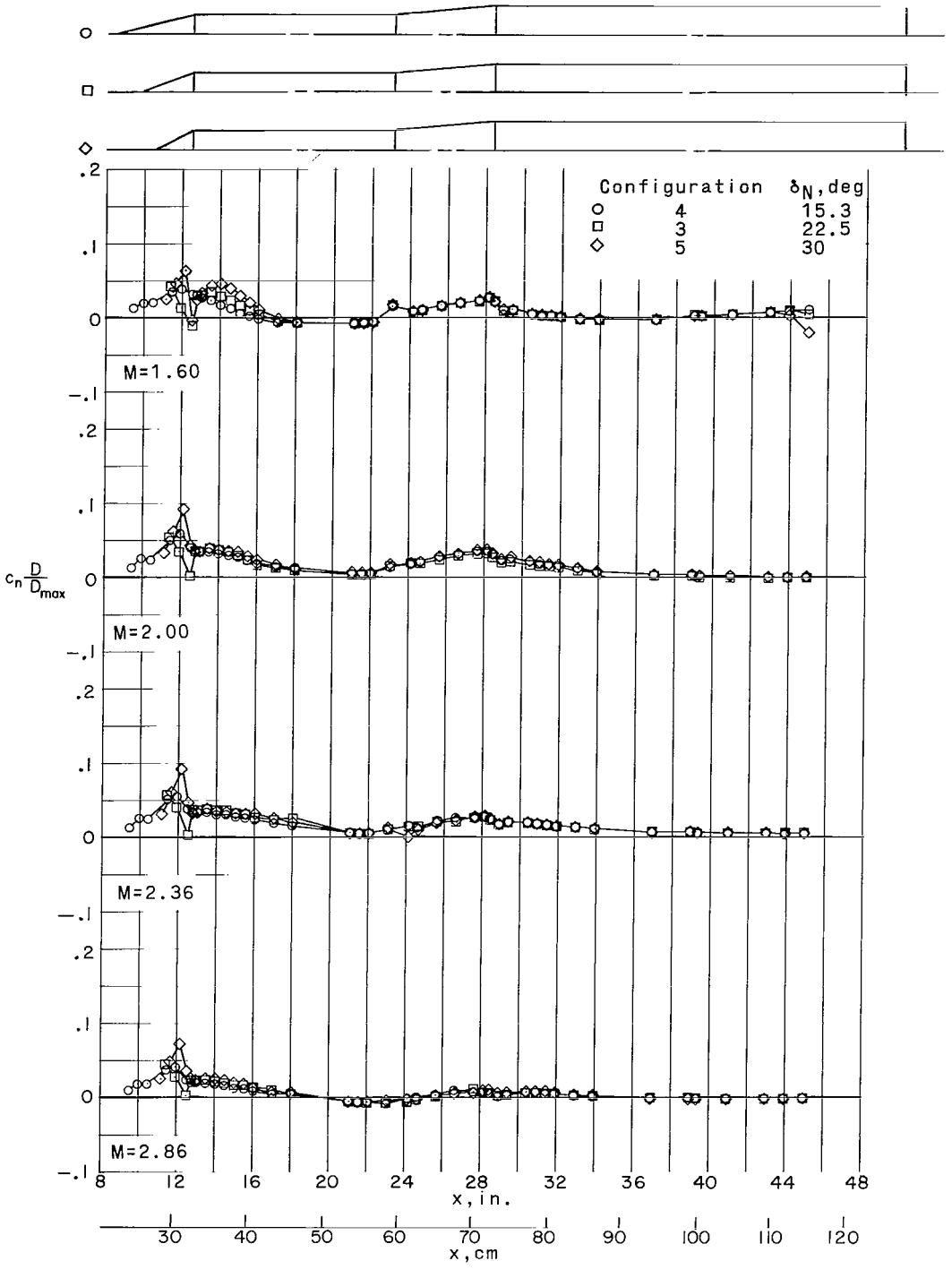

(a) $\alpha = 3^{0}$.

Figure 8.- Effects of variations in nose-cone angle on launch vehicle section normal-force-coefficient distribution. $\delta_F = 5^{0}$.

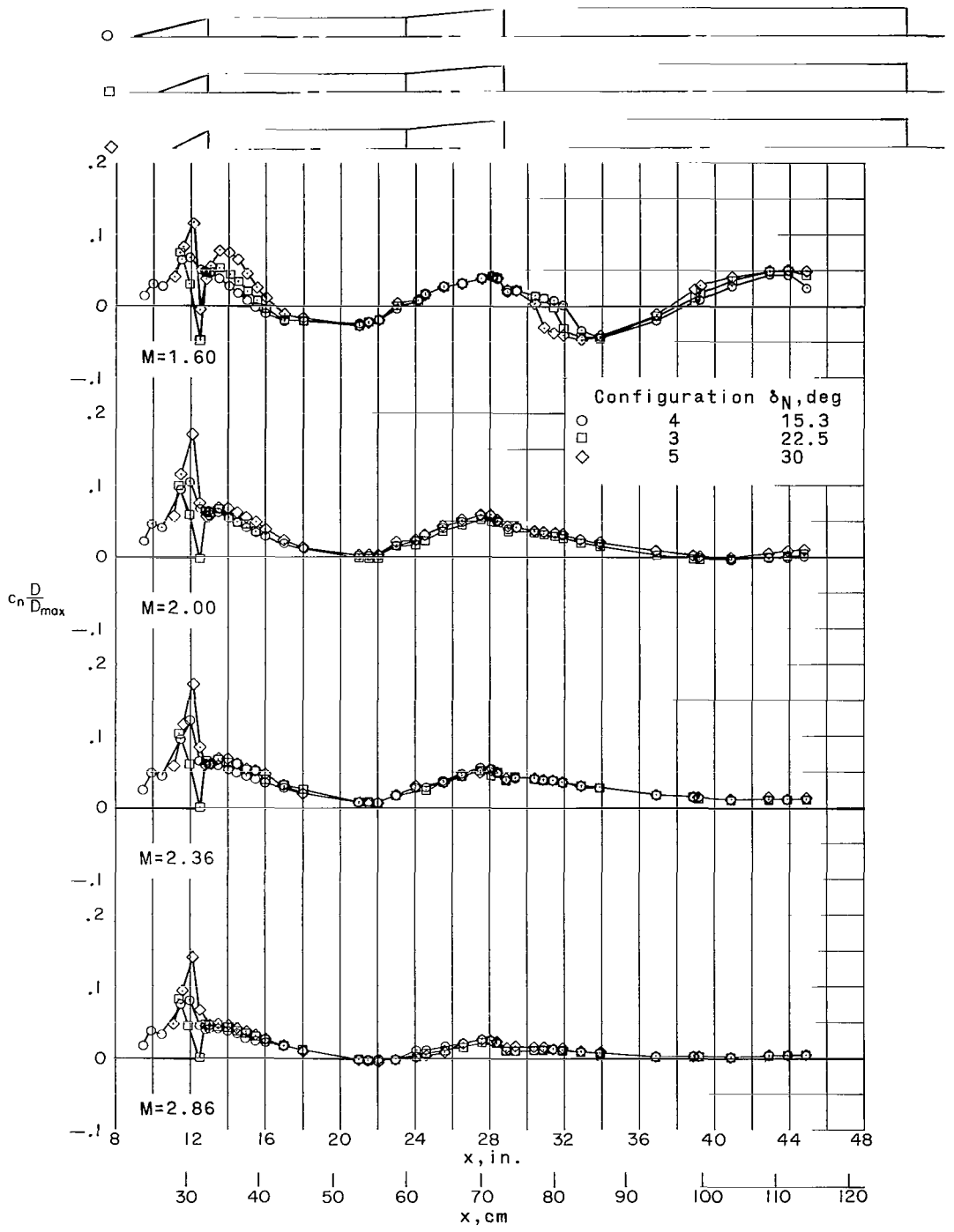

(b) $\alpha = 6^{0}$.

Figure 8.- Concluded.

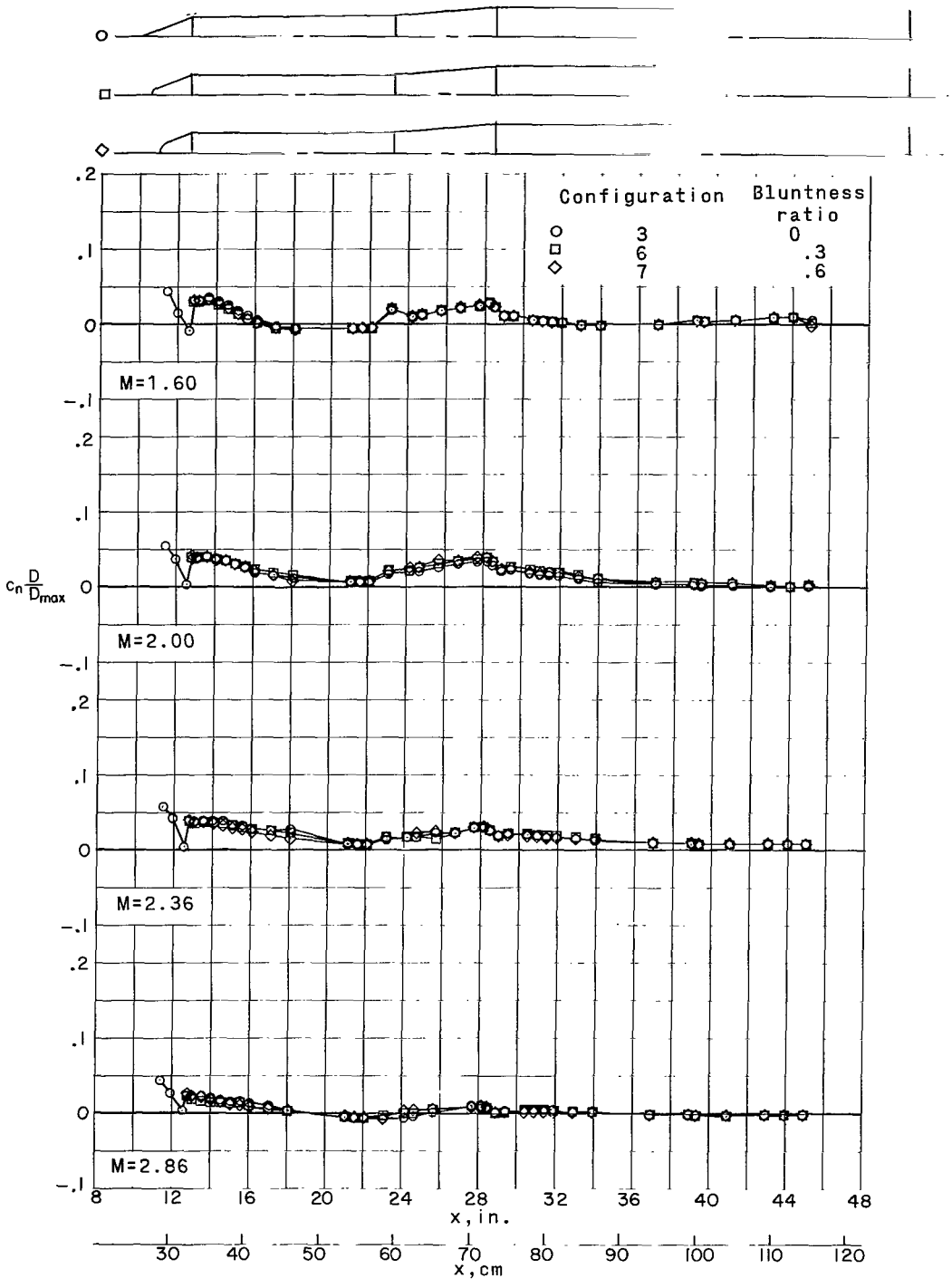

(a) $\alpha = 3^0$.

Figure 9.- Effects of nose-cone bluntness on launch vehicle section normal-force-coefficient distribution. $\delta_N = 22.5^0$; $\delta_F = 5^0$.

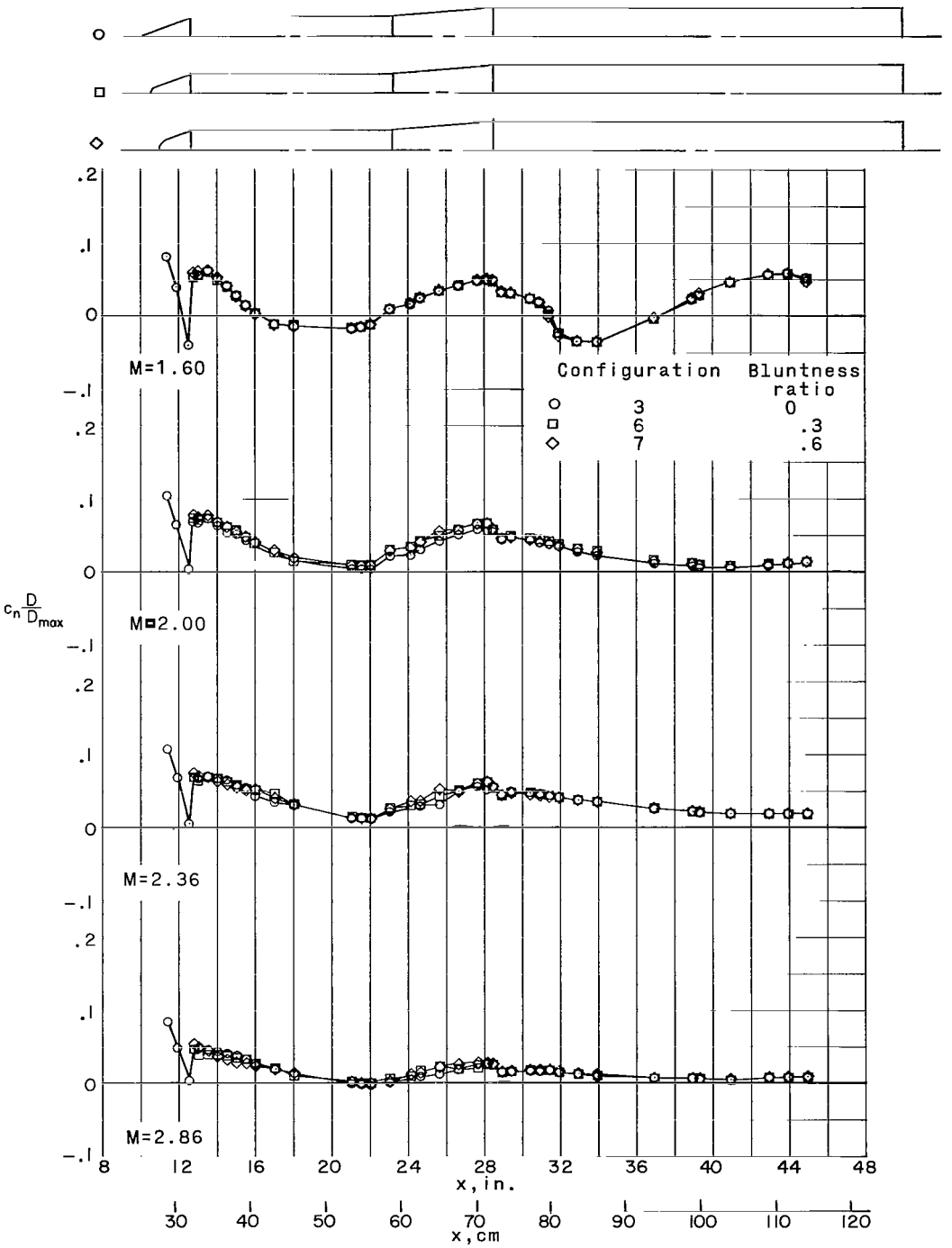

(b) $\alpha = 6^0$.

Figure 9.- Concluded.

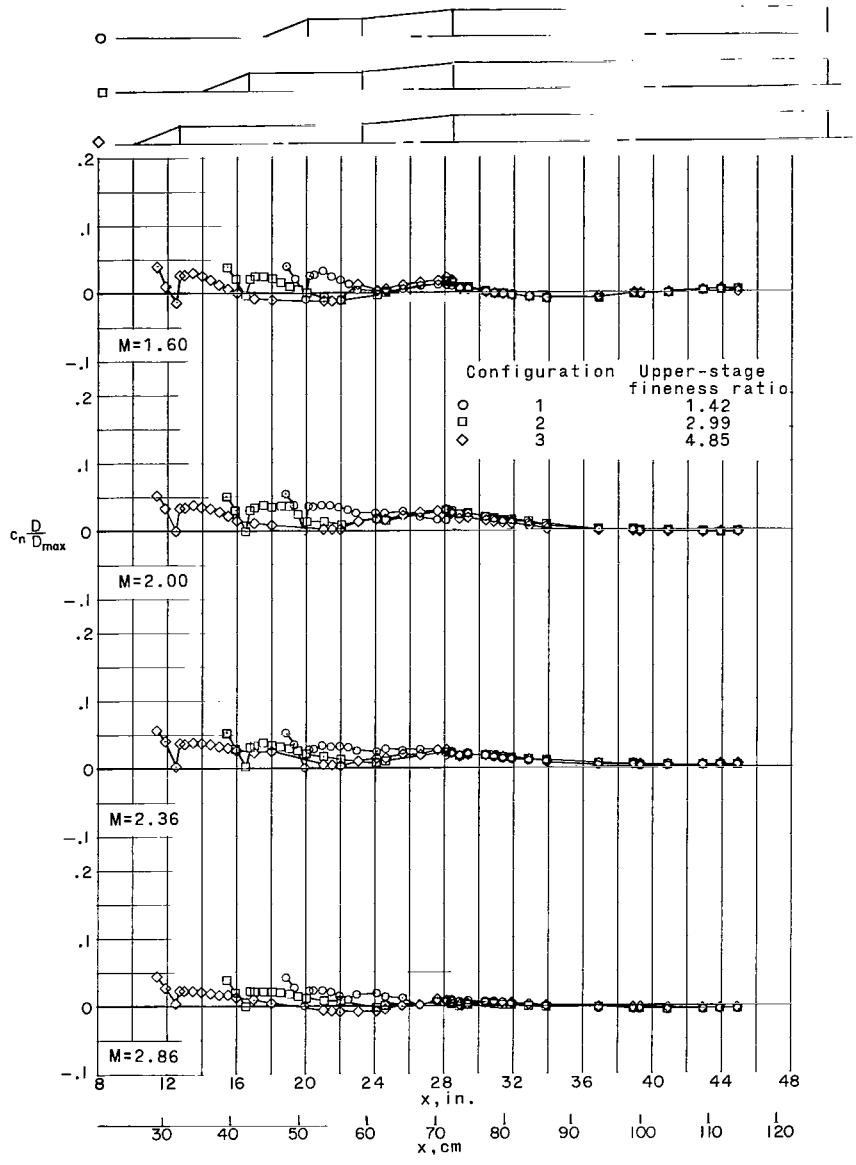

(a) $\alpha = 3^0$.

Figure 10.- Effects of variations in upper-stage fineness ratio on launch vehicle section normal-force-coefficient distribution. $\delta_N = 22.5^0$; $\delta_F = 5^0$.

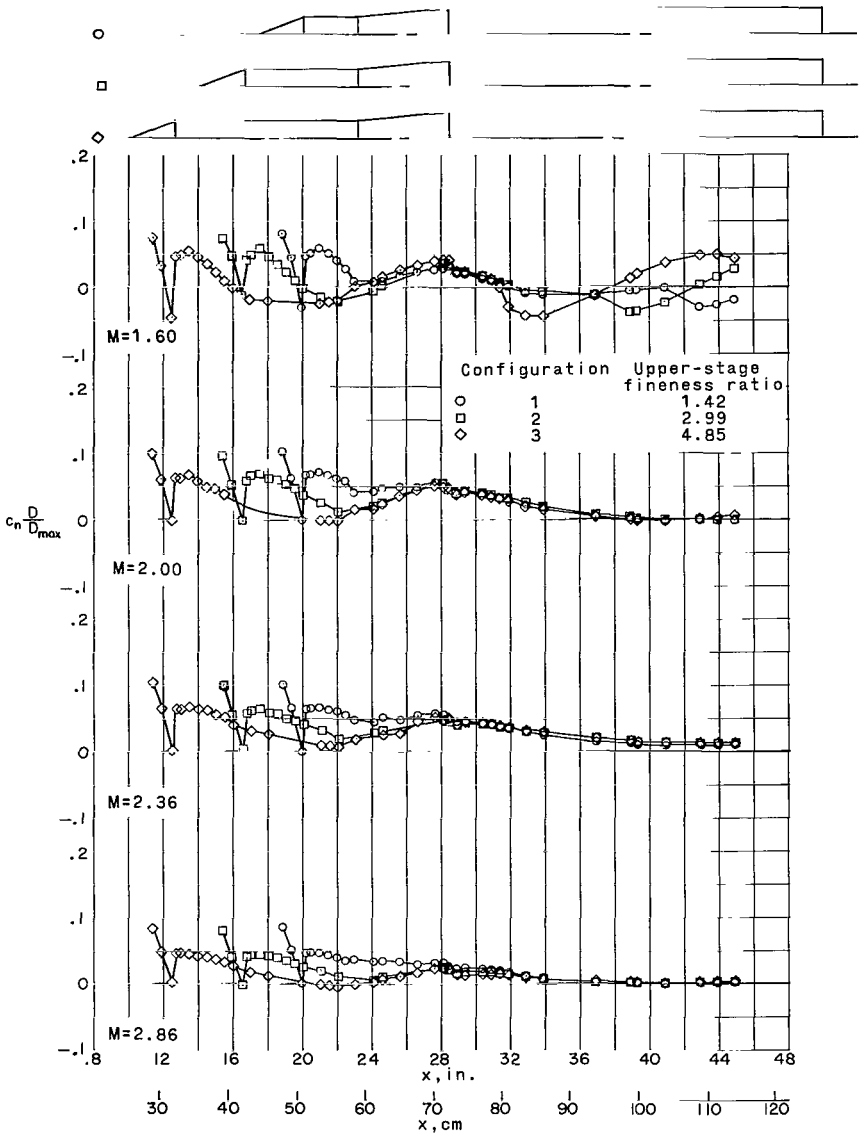

(b) $\alpha = 6^0$.

Figure 10.- Concluded.

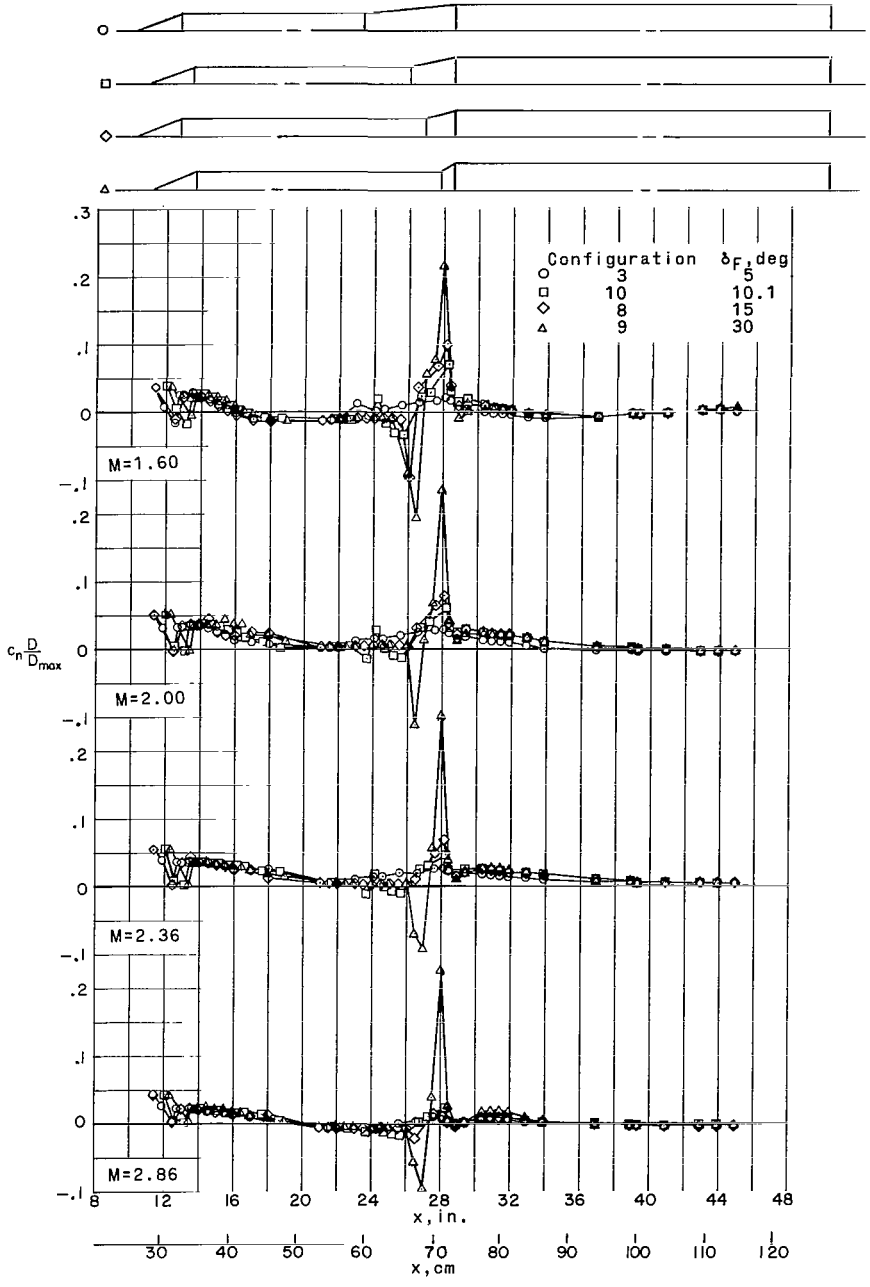

(a) $\alpha = 3^0$.

Figure 11.- Effects of variations in stage transition-flare angle on launch vehicle section normal-force-coefficient distribution. $\delta_N = 22.5^0$.

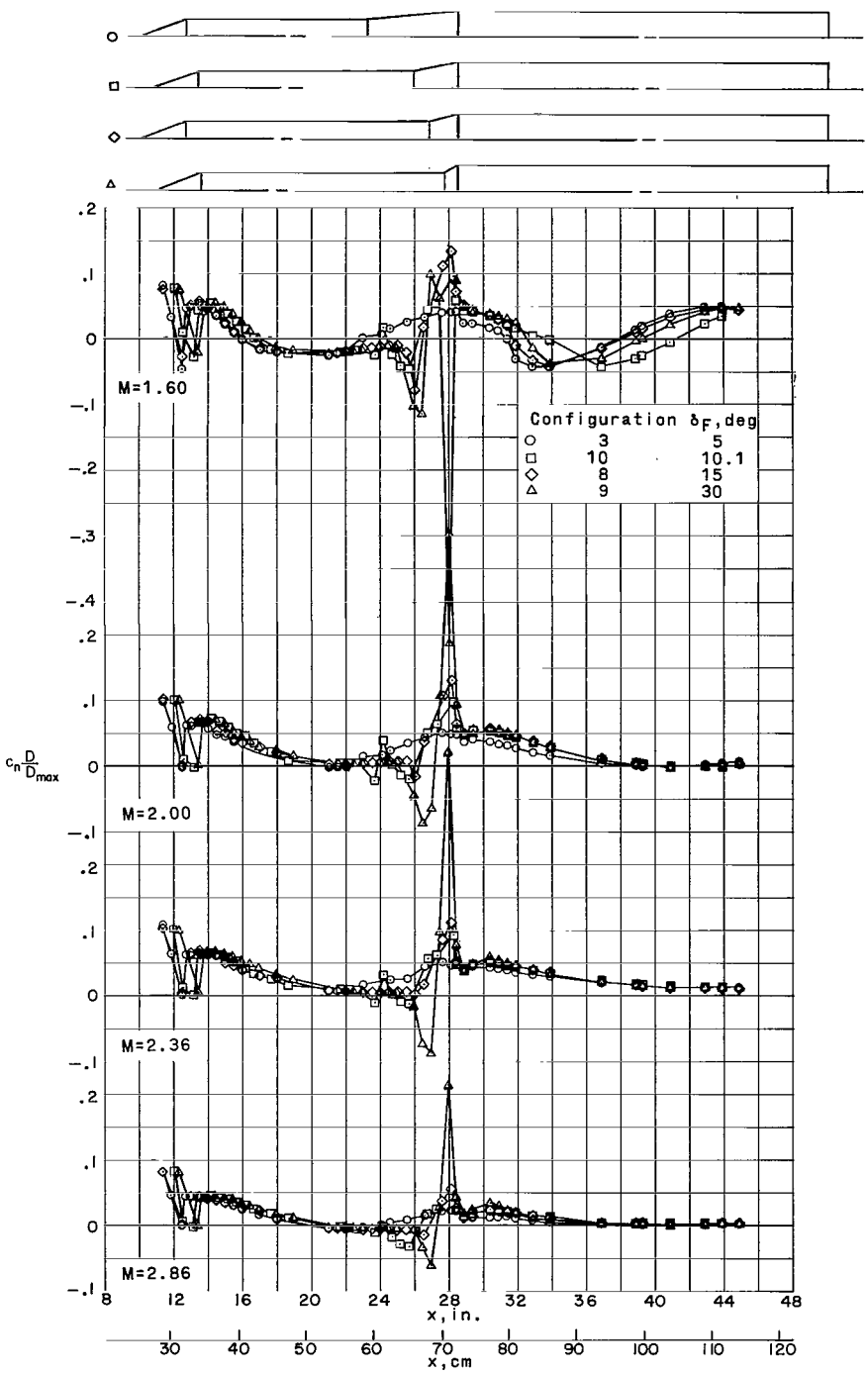

(b) $\alpha = 6^0$.

Figure 11.- Concluded.

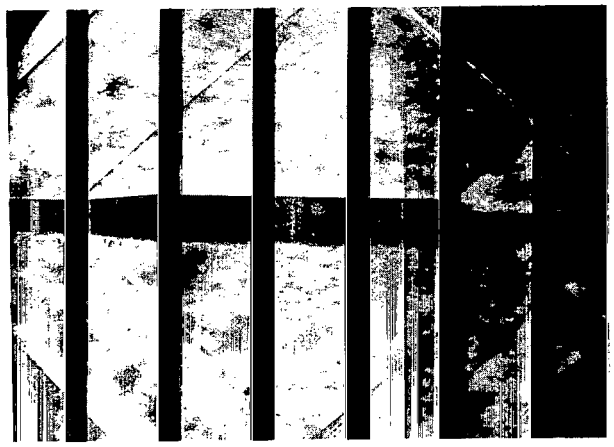

Configuration 3, δ_F=5°

Configuration 10, δ_F=10.1°

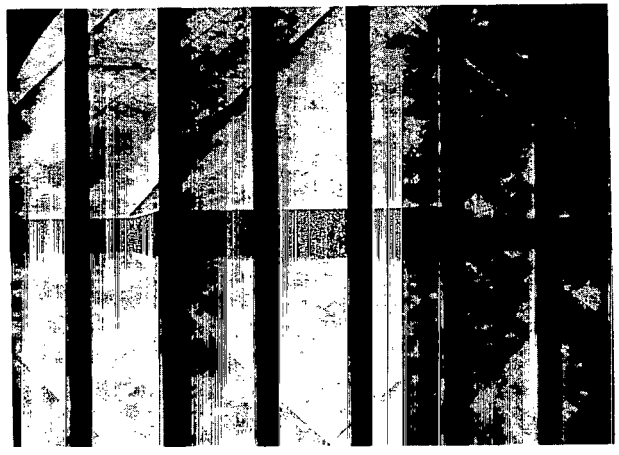

Configuration 8, δ_F=15°

Configuration 9, δ_F=30°

(a) $\alpha \approx 0^0$.

L-66-1137

Figure 12.- Schlieren photographs of models with variations in transition-flare angle. $\delta_N = 22.5^0$; M = 1.

Configuration 3, δ_F=5°

Configuration 10, δ_F=10.1°

Configuration 8, δ_F=15°

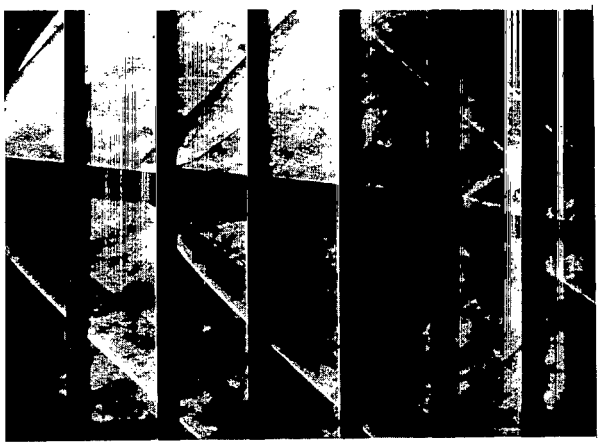

Configuration 9, δ_F=30°

(b) $\alpha \approx 6^0$.

L-66-1138

Figure 12.- Concluded.

"The aeronautical and space activities of the United States shall be conducted so as to contribute . . . to the expansion of human knowledge of phenomena in the atmosphere and space. The Administration shall provide for the widest practicable and appropriate dissemination of information concerning its activities and the results thereof."

—NATIONAL AERONAUTICS AND SPACE ACT OF 1958

NASA SCIENTIFIC AND TECHNICAL PUBLICATIONS

TECHNICAL REPORTS: Scientific and technical information considered important, complete, and a lasting contribution to existing knowledge.

TECHNICAL NOTES: Information less broad in scope but nevertheless of importance as a contribution to existing knowledge.

TECHNICAL MEMORANDUMS: Information receiving limited distribution because of preliminary data, security classification, or other reasons.

CONTRACTOR REPORTS: Technical information generated in connection with a NASA contract or grant and released under NASA auspices.

TECHNICAL TRANSLATIONS: Information published in a foreign language considered to merit NASA distribution in English.

TECHNICAL REPRINTS: Information derived from NASA activities and initially published in the form of journal articles.

SPECIAL PUBLICATIONS: Information derived from or of value to NASA activities but not necessarily reporting the results of individual NASA-programmed scientific efforts. Publications include conference proceedings, monographs, data compilations, handbooks, sourcebooks, and special bibliographies.

Details on the availability of these publications may be obtained from:

SCIENTIFIC AND TECHNICAL INFORMATION DIVISION

NATIONAL AERONAUTICS AND SPACE ADMINISTRATION

Washington, D.C. 20546